Vortex pinning and non-Hermitian quantum mechanics

Naomichi Hatano*
Lyman Laboratory of Physics, Harvard University, Cambridge, Massachusetts 02138
and Department of Physics, University of Tokyo, Hongo, Bunkyo, Tokyo 113, Japan

David R. Nelson
Lyman Laboratory of Physics, Harvard University, Cambridge, Massachusetts 02138
(Received 16 May 1997)

A delocalization phenomenon is studied in a class of non-Hermitian random quantum-mechanical problems. Delocalization arises in response to a sufficiently large constant imaginary vector potential. The transition is related to depinning of flux lines from extended defects in type-II superconductors subject to a tilted external magnetic field. The physical meaning of the complex eigenvalues and currents of the non-Hermitian system is elucidated in terms of properties of tilted vortex lines. The singular behavior of the penetration length describing stretched exponential screening of a perpendicular magnetic field (transverse Meissner effect), the surface transverse magnetization, and the trapping length is determined near the flux-line depinning point. [S0163-1829(97)03438-3]

I. INTRODUCTION

Although Hamiltonians must be Hermitian in conventional quantum mechanics, non-Hermitian operators do appear in other physical contexts: The time evolution of non-Hermitian Liouville operators can describe various nonequilibrium processes;[1–3] the transfer matrix of two-dimensional asymmetric vertex models leads to non-Hermitian Hamiltonians for quantum spin chains.[4]

In the present paper we investigate localization phenomena in an especially simple class of *random* non-Hermitian Hamiltonians. Although non-Hermitian, our problem is sufficiently close to conventional quantum mechanics that it will be convenient to use a quantum language to describe the results. Specifically, we show that a delocalization transition occurs (even in one and two dimensions) in the following one-body Hamiltonians in d dimensions: first, the Hamiltonian in continuum space

$$\mathcal{H} \equiv \frac{(\mathbf{p}+i\mathbf{g})^2}{2m} + V(\mathbf{x}), \tag{1.1}$$

where $\mathbf{p}=(h/i)\partial/\partial\mathbf{x}$ is the momentum operator and $V(\mathbf{x})$ is a random potential; second, the second-quantized lattice Hamiltonian, namely, the non-Hermitian Anderson model on a hypercubic lattice

$$\mathcal{H} \equiv -\frac{t}{2}\sum_{\mathbf{x}}\sum_{\nu=1}^{d}\left(e^{\mathbf{g}\cdot\mathbf{e}_\nu/\hbar}b^\dagger_{\mathbf{x}+\mathbf{e}_\nu}b_{\mathbf{x}}+e^{-\mathbf{g}\cdot\mathbf{e}_\nu/\hbar}b^\dagger_{\mathbf{x}}b_{\mathbf{x}+\mathbf{e}_\nu}\right) + \sum_{\mathbf{x}} V_{\mathbf{x}}b^\dagger_{\mathbf{x}}b_{\mathbf{x}}, \tag{1.2}$$

where the vectors $\{\mathbf{e}_\nu\}$ are the unit lattice vectors, the $\{b^\dagger_{\mathbf{x}}, b_{\mathbf{x}}\}$ are (boson) creation and annihilation operators, and $V_{\mathbf{x}}$ is a random potential. In both of the Hamiltonians, $\mathbf{g}$ is a non-Hermitian external field. Although the bulk of our discussion will concentrate on the properties of the single-particle Hamiltonians (1.1) and (1.2), many of our results will be relevant for *interacting* many-body boson problems, provided that we forbid double occupancy of eigenstates in the localized regime.[5] Interaction effects in both the localized and delocalized phases will be discussed in Sec. VIII.

We can regard the non-Hermitian field as an imaginary vector potential. Models with a real gauge field $\mathbf{A}$ would be written in the Hermitian forms

$$\mathcal{H}' = \frac{(\mathbf{p}-e\mathbf{A})^2}{2m} + V(\mathbf{x}) \tag{1.3}$$

and

$$\mathcal{H}' = -\frac{t}{2}\sum_{\mathbf{x}}\sum_{\nu=1}^{d}\left(e^{ie\mathbf{A}\cdot\mathbf{e}_\nu/\hbar}b^\dagger_{\mathbf{x}+\mathbf{e}_\nu}b_{\mathbf{x}}+e^{-ie\mathbf{A}\cdot\mathbf{e}_\nu/\hbar}b^\dagger_{\mathbf{x}}b_{\mathbf{x}+\mathbf{e}_\nu}\right) + \sum_{\mathbf{x}} V_{\mathbf{x}}b^\dagger_{\mathbf{x}}b_{\mathbf{x}}. \tag{1.4}$$

In two dimensions with spatially varying $\mathbf{A}=\mathbf{A}(\mathbf{x})$, these Hamiltonians describe the quantum Hall system, where some of the localized states of the $\mathbf{A}=\mathbf{0}$ case are delocalized in the presence of the gauge field.[6] We obtain the non-Hermitian Hamiltonians (1.1) and (1.2) by replacing $-e\mathbf{A}(\mathbf{x})$ with a constant $i\mathbf{g}$. In this non-Hermitian case, we show that *all* eigenstates can be delocalized (even in one dimension) for large $\mathbf{g}$.

This problem has direct physical relevance when we map the non-Hermitian quantum system in d dimensions to a problem of classical equilibrium statistical mechanics in $d+1$ dimensions. Consider a matrix element of the imaginary-time-evolution operator

$$\mathcal{Z} = \langle \psi^f | e^{-L_\tau \mathcal{H}/\hbar} | \psi^i \rangle, \tag{1.5}$$

where the Hamiltonian $\mathcal{H}$ is given by Eq. (1.1). The bra and ket vectors are the initial and final states, respectively. Using

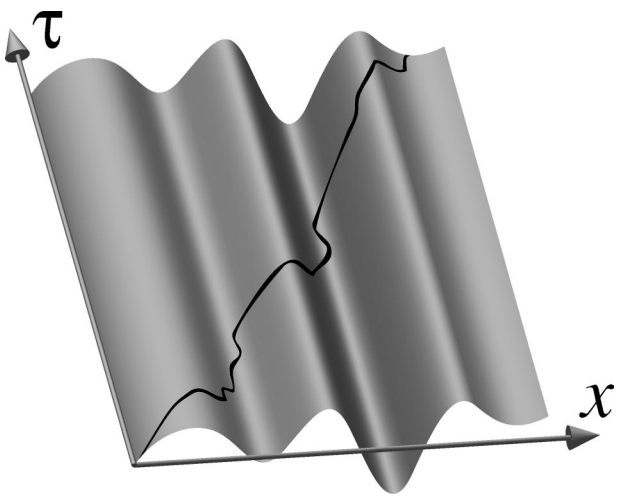

FIG. 1. Situation described by the classical Hamiltonian (1.7) in $1+1$ dimensions. The wavy line indicates a tilted string with a single-valued trajectory $x(\tau)$ subject to thermal fluctuations.

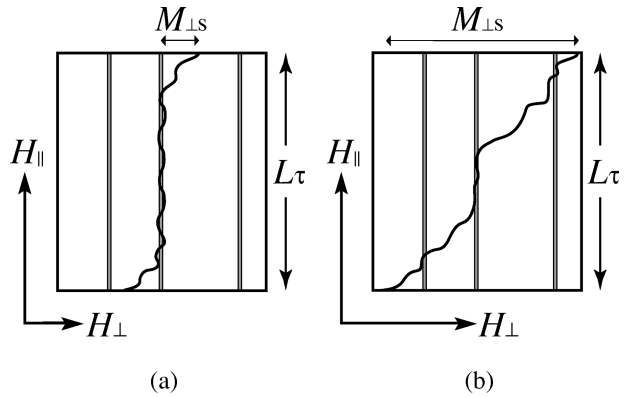

FIG. 2. Flux-line depinning from a columnar defect in a superconductor: (a) the bulk part of the flux line is pinned by the defect and the transverse magnetization has a contribution only from the *surface* transverse magnetization $M_{\perp s}$; (b) the flux line is depinned and the ''surface'' transverse magnetization now has a macroscopic value $M_{\perp s} \propto L_\tau$, where L_τ is the thickness of the sample.

the standard path-integral scheme, we can express the above matrix element as the partition function

$$\mathcal{Z} = \int \mathcal{D}\mathbf{x}\, e^{-E_{\rm cl}[\mathbf{x}(\tau)]/\hbar}, \tag{1.6}$$

where $\int \mathcal{D}\mathbf{x}$ denotes summation over all possible world-line configurations $\mathbf{x}(\tau)$ and $E_{\rm cl}$ is the energy of a classical elastic string in $d+1$ dimensions, given by

$$E_{\rm cl}[\mathbf{x}(\tau)] \equiv \int_0^{L_\tau} d\tau \left[\frac{m}{2} \left(\frac{d\mathbf{x}}{d\tau} \right)^2 - \mathbf{g} \cdot \frac{d\mathbf{x}}{d\tau} + V(\mathbf{x}) \right]. \tag{1.7}$$

The energy $E_{\rm cl}$ is of course the imaginary-time action for the equivalent quantum problem. The Planck parameter $\hbar$ is interpreted as the temperature of the classical system.

The above classical system expresses the following physics; see Fig. 1. Consider a thermally fluctuating string put on a *random* washboard potential. The first two terms of the Eq. (1.7) are optimized when the string is tilted from the τ direction by the angle $\theta \equiv \tan^{-1}(g/m)$. On the other hand, the potential tries to make the string parallel to the τ direction to take advantage of particularly deep valleys in the random potential. We might thus expect a depinning transition of the string from the random washboard potential with increasing g.

We suspect that there are many physical realizations of the above statistical-mechanical problem. For an application to population biology see Ref. 7. The present study is motivated particularly by a depinning transition of magnetic flux lines in type-II superconductors with quenched disorder. It has been recognized that impurities and defects play an essential role in the mixed phase of type-II superconductors. Flux lines, subject to electromagnetic forces due to applied currents, can move and dissipate energy, thus destroying the superconductivity, unless they are pinned by impurities or defects. In particular, extended defects such as columnar defects and twin boundaries pin flux lines parallel to them efficiently and thereby expand the region of zero resistance dramatically; see Refs. 8–10.

The situation described by the classical Hamiltonian (1.7) emerges when the external magnetic field generating the flux lines is not parallel to the extended defects; see Fig. 2. We may expect that the bulk part of the flux line remains pinned by the extended defects when the transverse component of the magnetic field $\mathbf{H}_\perp$ is weak. This phenomenon is called the *transverse Meissner effect*;[10] the system exhibits perfect bulk diamagnetism against $\mathbf{H}_\perp$ for a slightly tilted magnetic field. When we increase $\mathbf{H}_\perp$, i.e., tilt the magnetic field further relative to the extended defects, a depinning transition takes place at a certain strength of the transverse field, namely, $H_{\perp c}$. We note that randomness in the potential is essential for the transverse Meissner effect to work at finite temperatures. For a periodic potential, thermally activated kinks always lead to *extended* eigenfunctions in the equivalent quantum problem (Bloch's theorem) and the effect vanishes. See Ref. 11 for a discussion.

Nelson and Vinokur[10] have described flux-line pinning by means of the path-integral scheme. They mapped a phenomenological Hamiltonian for flux lines with extended defects onto interacting bosons in $2+1$ dimensions with point impurities. A low-temperature phase with flux lines localized on extended defects was related to the Bose-glass phase[12] of disordered boson systems. When the applied magnetic field is tilted away from the extended defects, the corresponding boson problem acquires the non-Hermitian field $\mathbf{g}$.[13,5] The flux-line depinning transition due to the magnetic-field tilt corresponds to a delocalization transition of the non-Hermitian quantum problem. The expected T-$H_\perp$ phase diagram of the flux-line system (with $\mathbf{H}_\parallel$, the field component parallel to the columns, held fixed) is shown in Fig. 3.[10] The transition to a flux-liquid or ''superfluid'' phase with increasing temperature for $\mathbf{H}_\perp = \mathbf{0}$ is of the usual Bose-glass type.[12] In the present paper we shall focus on the transition curves for $\mathbf{H}_\perp \neq \mathbf{0}$. Hence we fix the temperature and follow the trajectory of increasing $\mathbf{H}_\perp$, indicated in Fig. 3 as a thick arrow. We first describe the delocalization transition of the non-Hermitian quantum problem and next translate the results into the language of flux-line depinning. We mainly discuss the one-body (or one-flux-line) problem of the non-Hermitian quantum mechanics. Some of our results were summarized in a previous publication.[5]

One advantage of discussing the flux-line depinning in

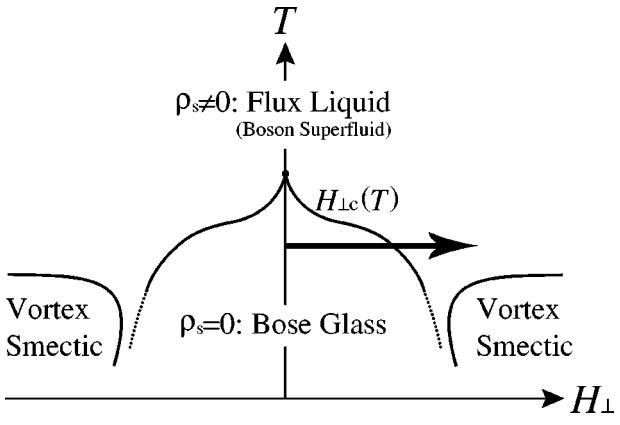

FIG. 3. Schematic phase diagram of high-temperature superconductors with columnar defects (Ref. 10). The abscissa indicates the transverse component of the external magnetic field.

terms of an equivalent ''quantum'' system comes from the fact that many ideas are already available concerning localization in Hermitian random systems, such as the Anderson transition and Mott's variable-range hopping. Our problem is perhaps the simplest non-Hermitian generalization of these phenomena. The inverse localization length of a wave function, when it delocalizes, is proportional to the critical transverse field $H_{\perp c}$. As $\mathbf{H}_\perp$ increases, a precursor of the flux-line depinning appears first near the surface of the superconductor. Slightly below the critical point the ends of the pinned flux line begin to tear free from the pinning center. Thus the transverse Meissner effect first breaks down near the surfaces and the typical depth of the region where this bending takes place is a ''penetration depth'' (*different* from the penetration depth associated with the underlying superconducting material) that accompanies the transverse Meissner effect. A Mott variable-range-hopping description of this depinning will lead us to the conclusion that the penetration depth τ^* diverges at the transition point $H_{\perp c}$ as

$$\tau^* \sim (H_{\perp c} - H_\perp)^{-2} \tag{1.8}$$

for the random columnar defects and

$$\tau^* \sim (H_{\perp c} - H_\perp)^{-1} \tag{1.9}$$

for the random twin boundaries. The pinning becomes ineffective above the critical field. The direction of the bulk transverse magnetization jumps at the critical point, while the surface transverse magnetization diverges in both cases according to

$$M_{\perp s} \sim (H_{\perp c} - H_\perp)^{-1}. \tag{1.10}$$

We find *stretched-exponential* relaxation of the perpendicular magnetization to zero as one goes deep into the bulk of the sample from the surface.

The penetration depth τ^* may be observed experimentally by measuring the response to an ac magnetic field superimposed on the dc field $\mathbf{H}_\perp$; only the dangling ends of the flux lines will respond to the ac field and the length of these line segments diverges at the transition. It would be interesting to check our prediction of a diverging penetration depth near the Bose-glass transition with such an experiment.

A preliminary account of this work appeared in Ref. 5. For a related problem that arises from the physics of charge-density waves, with some results applicable to vortex lines, see Ref. 14. See Ref. 15 for a related problem in fluid mechanics.

The plan of this paper is as follows. Section II describes basic relations between the flux-line system and non-Hermitian quantum mechanics. In Sec. III we explain how the delocalization transition occurs in the non-Hermitian random system. We present solutions of non-Hermitian systems in Secs. IV–VI. The predictions for the transverse Meissner effect are derived in Sec. VII. Section VIII discusses the effect of interactions in the delocalized phase in both $1+1$ and $2+1$ dimensions.

II. FLUX LINES AND NON-HERMITIAN QUANTUM MECHANICS

In this section we review the basic correspondence between vortex lines in superconductors and the non-Hermitian quantum system (1.1). We then describe what the current and the wave functions of the non-Hermitian system mean for vortex trajectories.

A. Path-integral mapping

We start with the energy of a flux line in a $(d+1)$-dimensional type-II superconductor[10]

$$E_{\text{flux}} = \int_0^{L_\tau} d\tau \left(\frac{\tilde{\varepsilon}_1}{2} \left| \frac{d\mathbf{x}}{d\tau} \right|^2 + V(\mathbf{x}) - \frac{\phi_0 \mathbf{H}_\perp}{4\pi} \cdot \frac{d\mathbf{x}}{d\tau} \right). \tag{2.1}$$

This is a phenomenological Hamiltonian for the flux-line system where all columnar defects or twin boundaries are parallel. Here τ denotes the coordinate parallel to the extended defects, while $\mathbf{x}$ denotes the d-dimensional coordinates perpendicular to the defects. We describe the flux line as a single-valued function $\mathbf{x}(\tau)$ by neglecting overhangs of the flux line. The thickness of the superconductor in the τ direction is denoted by L_τ.

The first kinetic-energy-like term of the integrand in Eq. (2.1) comes from the harmonic approximation to the energy increase due to local tilt of the flux line. The ''mass,'' or tilt modulus, is denoted by $\tilde{\varepsilon}_1$. When using quantum language to describe this problem, we shall make the correspondence

$$\tilde{\varepsilon}_1 \leftrightarrow m. \tag{2.2}$$

The potential V is generated by columnar defects or twin boundaries. Each columnar defect is specified by a point $\mathbf{X}_k$ in the $\mathbf{x}$ plane. We assume that the columnar defects are distributed randomly:

$$V(\mathbf{x}) = \sum_{k=1}^{M} V_1(\mathbf{x} - \mathbf{X}_k), \tag{2.3}$$

where M denotes the number of columnar defects, V_1 is the potential of an individual defect, and $\mathbf{X}_k$ is the random position of the kth columnar defect. In the case of twin boundaries, we consider only the situation where all twins are parallel to each other. By projecting out the degree of freedom perpendicular to τ and parallel to the twin boundaries,[10,16] we

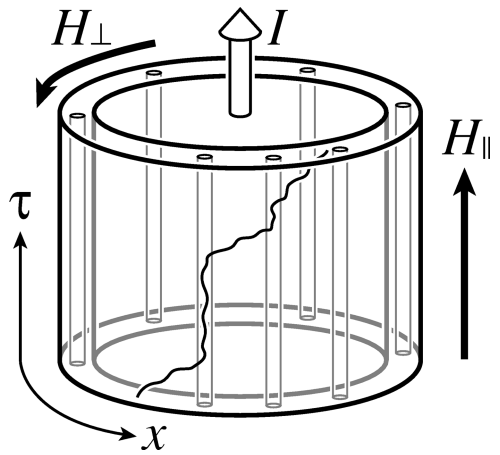

FIG. 4. One flux line (wavy curve) induced by the field $\mathbf{H}_\parallel$ and interacting with columnar defects in a cylindrical superconducting shell. The transverse component $\mathbf{H}_\perp$ is generated by the current $\mathbf{I}$ threading the ring.

can reduce the dimensionality of the $\mathbf{x}$ space by one. (We neglect effects due to an enhanced concentration of point disorder that may occur in twins.) Thus each twin boundary acts like a line defect in $1+1$ dimensions. In short, we can set $d=2$ for columnar defects and $d=1$ for twin boundaries.

The third term of the integrand in Eq. (2.1) is due to the transverse component of the magnetic field $\mathbf{H}_\perp$. The flux quantum $2\pi\hbar c/2e$ is denoted by ϕ_0. In the absence of a pinning potential, this term is optimized energetically when the flux line tilts to follow the external field.

Figure 4 shows a flux-line system described by the above phenomenology in $1+1$ dimensions with columnar pinning. We assume periodic boundary conditions in the $\mathbf{x}$ direction, although these could be replaced by reservoirs of flux lines at the edges of the sample. In this geometry, the transverse component $\mathbf{H}_\perp$ is generated by the current threading the cylinder of a thin superconductor. As we shall see, the physics resembles the Aharonov-Bohm experiment carried out on a mesoscopic quantum ring with, however, an *imaginary* ''flux'' through the ring.

The partition function of the flux-line system (2.1) is given by

$$\mathcal{Z}=\int \mathcal{D}\mathbf{x}\,\exp\left(-\frac{E_{\rm flux}}{k_BT}\right), \tag{2.4}$$

where $\int\mathcal{D}\mathbf{x}$ denotes integration over all possible configurations $\mathbf{x}(\tau)$ of the flux line. Upon identifying Eq. (2.4) with Eq. (1.6), we are led to a correspondence between the flux-line system (2.1) and the non-Hermitian quantum system (1.1) summarized in Table I. In particular, the thermal fluctuations of the flux-line system are equivalent to zero-point motion of the quantum system and

$$k_BT\leftrightarrow\hbar. \tag{2.5}$$

The tilt term in Eq. (2.1) is related to the non-Hermitian field in Eq. (1.1) by

$$\mathbf{g}\equiv\frac{\phi_0\mathbf{H}_\perp}{4\pi}. \tag{2.6}$$

Boundary conditions at the bottom and top surfaces of the superconductor are represented by the initial and final vectors of Eq. (1.5) in the forms

$$\langle\psi^f|\equiv\int d\mathbf{x}\langle\mathbf{x}|,\quad |\psi^i\rangle\equiv\int d\mathbf{x}|\mathbf{x}\rangle. \tag{2.7}$$

These boundary conditions in the imaginary-time direction mean that we integrate freely over the points where vortex lines enter and exit the sample.

Although the derivation of the quantum problem (1.1) from the classical elastic string described by Eq. (2.1) is straightforward in the path-integral scheme, it is also useful to think in terms of Galilean boosts.[13,17] We can eliminate the additional term in Eq. (2.1) by the Galilean transformation

$$\mathbf{x}'=\mathbf{x}-\mathbf{v}t,\quad t'=t, \tag{2.8}$$

where the velocity of the moving frame is

$$\mathbf{v}=\frac{\phi_0\mathbf{H}_\perp}{4\pi i\tilde{\varepsilon}_1}\equiv\frac{\mathbf{g}}{im}. \tag{2.9}$$

Note that the velocity is *imaginary* because of the imaginary time $t=i\tau$ in the equivalent quantum problem. The above Galilean transformation changes the kinetic term of the Hermitian Hamiltonian to the form

$$\frac{\mathbf{p}^2}{2m}\rightarrow\frac{(\mathbf{p}-m\mathbf{v})^2}{2m}, \tag{2.10}$$

which results in the kinetic term in Eq. (1.1).

TABLE I. Correspondence between the $(d+1)$-dimensional flux-line system and the d-dimensional quantum system.

partition function (2.4)	partition function (1.5)
thickness L_τ	imaginary time τ
temperature k_BT	Planck parameter $\hbar$
tilt modulus $\tilde{\varepsilon}_1$	mass m
tilting field $\phi_0 H_\perp/(4\pi)$	Non-Hermitian field g
tilt slope $dx/d\tau$ (proportional to the transverse magnetization)	ImJ, where J is the current
probability distribution at $\tau=0$ $(L_\tau\rightarrow\infty)$	Left eigenvector $\psi^L(x)$
at $\tau=L_\tau$	Right eigenvector $\psi^R(x)$
at $\tau=L_\tau/2$	$\psi^L\psi^R$

We do not explicitly include interactions between flux lines in the Hamiltonian (2.1) nor in the quantum Hamiltonians (1.1) and (1.2). However, a strong short-range repulsive potential may be treated approximately by forbidding multiple occupancy of localized levels of the quantum Hamiltonian. Since the particle mapped from the flux line follows the Bose statistics,[10] we may treat many-flux-line problems as hard-core bosons in a random potential. For $d=1$, hard-core bosons are equivalent to fermions and hence we can use the Pauli principle directly to treat many-body problems in this case. See Sec. VIII for a discussion of interaction effects using a boson formalism in d dimensions.

B. Imaginary current and the transverse magnetization

We show in the following that the imaginary part of the current of the non-Hermitian system yields the average slope of a vortex trajectory as it crosses the sample. Since the non-Hermitian field $\mathbf{g}$ acts like an imaginary vector potential, we define the current operator as

$$\mathbf{J}\equiv -i\frac{\partial\mathcal{H}}{\partial\mathbf{g}}=\frac{\mathbf{p}+i\mathbf{g}}{m}=\mathbf{J}_{\rm para}+\mathbf{J}_{\rm dia}, \tag{2.11}$$

where

$$\mathbf{J}_{\rm para}\equiv\frac{\mathbf{p}}{m},\quad \mathbf{J}_{\rm dia}\equiv i\frac{\mathbf{g}}{m}. \tag{2.12}$$

Note first that the expectation value of the position of the flux line at the distance τ from the bottom surface of the superconductor is given by

$$\langle\mathbf{x}\rangle_\tau\equiv\frac{1}{\mathcal{Z}}\langle\psi^f|e^{-(L_\tau-\tau)\mathcal{H}/\hbar}\mathbf{x}^{\rm op}e^{-\tau\mathcal{H}/\hbar}|\psi^i\rangle, \tag{2.13}$$

where the partition function $\mathcal{Z}$ is defined by Eq. (1.5) and $\mathbf{x}^{\rm op}$ is the position operator acting on position eigenstates $|\mathbf{x}\rangle$ such that $\mathbf{x}^{\rm op}|\mathbf{x}\rangle=\mathbf{x}|\mathbf{x}\rangle$. Note also the useful commutation relation

$$[\mathcal{H},\mathbf{x}^{\rm op}]=-i\hbar\mathbf{J}, \tag{2.14}$$

which leads immediately to

$$\begin{aligned}\frac{\partial}{\partial\tau}\langle\mathbf{x}\rangle_\tau&=\frac{1}{\hbar\mathcal{Z}}\langle\psi^f|e^{-(L_\tau-\tau)\mathcal{H}/\hbar}[\mathcal{H},\mathbf{x}^{\rm op}]e^{-\tau\mathcal{H}/\hbar}|\psi^i\rangle\\&=-i\langle\mathbf{J}\rangle_\tau=\mathrm{Im}\langle\mathbf{J}\rangle_\tau.\end{aligned} \tag{2.15}$$

In the last line of Eq. (2.15), we used the fact that the expectation value of the current is pure imaginary in the present problem. The current carried by an individual eigenstate is *not* necessarily pure imaginary, where the current of a state ε_n is defined by

$$\mathbf{J}_n\equiv -i\frac{\partial\varepsilon_n}{\partial\mathbf{g}}. \tag{2.16}$$

However, a purely imaginary expectation value of the current arises owing to a pairing property of eigenvalues and eigenfunctions: if there is a complex eigenvalue ε with a right eigenvector ψ^R for this non-Hermitian problem, there is also the eigenvalue ε^* with the right eigenvector $(\psi^R)^*$. When we sum Eq. (2.16) over all the eigenstates to calculate the expectation value, the real part of the current of a state cancels out in a pairwise fashion.

The transverse component of the magnetization per vortex line at depth τ below the surface of the sample is proportional to the tilt slope:

$$\mathbf{m}_\perp(\tau)\equiv\frac{\partial}{\partial\tau}\langle\mathbf{x}\rangle_\tau=\mathrm{Im}\langle\mathbf{J}\rangle_\tau. \tag{2.17}$$

The total transverse magnetization is proportional to the net displacement of the flux line per unit length between the bottom surface ($\tau=0$) and the top surface ($\tau=L_\tau$):

$$\begin{aligned}\mathbf{M}_\perp\equiv n_v\frac{\phi_0}{L_\tau}\int_0^{L_\tau}\mathbf{m}_\perp(\tau)d\tau&=\frac{\phi_0 n_v}{L_\tau}\,\mathrm{Im}\int_0^{L_\tau}d\tau\langle\mathbf{J}\rangle_\tau\\&=\frac{\phi_0 n_v}{L_\tau}(\langle\mathbf{x}\rangle_{L_\tau}-\langle\mathbf{x}\rangle_0),\end{aligned} \tag{2.18}$$

where n_v is the density of vortices. As we show below, the last factor in the parentheses is given by

$$\langle\mathbf{x}\rangle_{L_\tau}-\langle\mathbf{x}\rangle_0=\hbar\frac{\partial}{\partial\mathbf{g}}\ln\mathcal{Z}. \tag{2.19}$$

Equation (2.18) is an indicator of the delocalization transition; the transverse magnetization must remain finite in the limit $L_\tau\to\infty$ in a depinned phase, while it must vanish macroscopically in a pinned glassy phase, which is the transverse Meissner effect. In fact, we show later that the vortex tilt $\mathbf{m}_\perp(\tau)$ appears only close to surfaces in the pinning regime and thus $\mathbf{M}_\perp$ vanishes as $L_\tau\to\infty$. In the limit $L_\tau\to\infty$, Eq. (2.19) becomes

$$\lim_{L_\tau\to\infty}(\langle\mathbf{x}\rangle_{L_\tau}-\langle\mathbf{x}\rangle_0)=-L_\tau\frac{\partial\varepsilon_{\rm g.s.}}{\partial\mathbf{g}}, \tag{2.20}$$

where $\varepsilon_{\rm g.s.}$ denotes the ground-state energy of $\mathcal{H}(\mathbf{g})$. (The ground state is defined by the lowest *real* part of the eigenenergy.[18]) Hence, in the pinning regime, the ground-state energy must be independent of $\mathbf{g}$. In the depinning regime, $-\partial\varepsilon_{\rm g.s.}/\partial\mathbf{g}$ is nonzero and equals the mean tilt slope of the corresponding flux line.

To prove Eq. (2.19), we proceed as follows. As stated above, the non-Hermitian field $\mathbf{g}$ acts like an imaginary vector potential. Because of this, we can gauge away the non-Hermitian field by applying the imaginary gauge transformation to the non-Hermitian Hamiltonian (1.1):

$$\mathcal{U}^{-1}\mathcal{H}(\mathbf{g})\mathcal{U}=\mathcal{H}(\mathbf{0}), \tag{2.21}$$

where

$$\mathcal{U}\equiv\exp\left(\frac{\mathbf{g}\cdot\mathbf{x}^{\rm op}}{\hbar}\right). \tag{2.22}$$

[This is just another expression of the Galilean transformation (2.10).] Therefore, we have

$$e^{-L_\tau\mathcal{H}(\mathbf{g})/\hbar}=\mathcal{U}e^{-L_\tau\mathcal{H}(\mathbf{0})/\hbar}\mathcal{U}^{-1} \tag{2.23}$$

and

$$\hbar \frac{\partial}{\partial \mathbf{g}} e^{-L_\tau \mathcal{H}(\mathbf{g})/\hbar} = \mathbf{x}^{\mathrm{op}} e^{-L_\tau \mathcal{H}(\mathbf{g})/\hbar} - e^{-L_\tau \mathcal{H}(\mathbf{g})/\hbar} \mathbf{x}^{\mathrm{op}}. \tag{2.24}$$

Upon taking thermodynamic averages (expectation values in quantum language), we obtain Eq. (2.19).

A conductivitylike transport coefficient may be defined by

$$\sigma_{\mu\nu} \equiv -i \frac{\partial}{\partial g_\nu} \langle J_\mu \rangle. \tag{2.25}$$

The quantity defined for each eigenstate

$$\sigma_{\mu\nu}^{(n)} \equiv -\frac{\partial^2 \varepsilon_n}{\partial g_\mu \partial g_\nu} \tag{2.26}$$

is a measure of the stiffness of the eigenfunction. In many-body problems, $\sigma_{\mu\nu}$ is related to the superfluid density of the relevant boson system.[19]

C. Probability distribution of a flux line and eigenvectors of the non-Hermitian Hamiltonian

We now outline the correspondence between the probability distribution of a flux line and the eigenvectors of the quantum system. The flux line fluctuates because of thermal excitations. This thermal agitation is described by quantum fluctuations of the corresponding fictitious non-Hermitian quantum particle. The probability distribution of the flux line due to thermal fluctuation is thus related to wave functions of the quantum system.

The probability distribution of the flux line at the distance τ from the bottom surface is given by[10]

$$P(\mathbf{x};\tau) \equiv \frac{1}{\mathcal{Z}} \langle \psi^f | e^{-(L_\tau - \tau)\mathcal{H}/\hbar} | \mathbf{x} \rangle \langle \mathbf{x} | e^{-\tau \mathcal{H}/\hbar} | \psi^i \rangle, \tag{2.27}$$

so that we can rewrite Eq. (2.13) as

$$\langle \mathbf{x} \rangle_\tau = \int \mathbf{x}\, P(\mathbf{x};\tau) d^d \mathbf{x}. \tag{2.28}$$

Let us calculate $P(\mathbf{x};\tau)$ in the limit $L_\tau \to \infty$. In this limit the exponential operator $\exp(-L_\tau \mathcal{H}/\hbar)$ can be approximated by

$$\lim_{L_\tau \to \infty} e^{-L_\tau \mathcal{H}/\hbar} \simeq |\psi_{\mathrm{g.s.}}\rangle e^{-L_\tau \varepsilon_{\mathrm{g.s.}}/\hbar} \langle \psi_{\mathrm{g.s.}}|. \tag{2.29}$$

Note here that left and right eigenvectors may be expressed as

$$\psi^R(\mathbf{x}) = \langle \mathbf{x} | \psi \rangle, \quad \psi^L(\mathbf{x}) = \langle \psi | \mathbf{x} \rangle. \tag{2.30}$$

Upon combining Eqs. (2.27) and (2.29), we find

$$\lim_{L_\tau \to \infty} P(\mathbf{x};0) = \frac{\psi^L_{\mathrm{g.s.}}(\mathbf{x})}{\int \psi^L_{\mathrm{g.s.}}(\mathbf{x}) d^d \mathbf{x}}, \tag{2.31}$$

$$\lim_{L_\tau \to \infty} P(\mathbf{x};L_\tau) = \frac{\psi^R_{\mathrm{g.s.}}(\mathbf{x})}{\int \psi^R_{\mathrm{g.s.}}(\mathbf{x}) d^d \mathbf{x}}, \tag{2.32}$$

and

$$\lim_{L_\tau \to \infty} P(\mathbf{x};L_\tau/2) = \psi^L_{\mathrm{g.s.}}(\mathbf{x}) \psi^R_{\mathrm{g.s.}}(\mathbf{x}). \tag{2.33}$$

Since the ground-state wave function is positive definite, the distributions (2.31) and (2.32) are well defined.

We remark on the nature of the limit in Eq. (2.29). For one-impurity systems (see Sec. IV), corrections to the right-hand side of Eq. (2.29) are of order $\exp(-L_\tau \Delta\varepsilon)$, where $\Delta\varepsilon$ is the energy gap above the ground state. For random systems, the argument in Sec. VII yields corrections that vanish as a stretched exponential function of L_τ.

For a finite density of flux lines, we can treat a strong short-range repulsive potential approximately by forbidding multiple occupancy of localized levels of the quantum Hamiltonian.[10] We then fill up the localized levels in order of increasing energy up to a certain level $\varepsilon = \mu$. The system is now characterized by an average chemical potential $\mu = \mu(H_\parallel)$, where $H_\parallel$ is the external magnetic field along the τ axis. This chemical potential controls the flux-line density and separates occupied and unoccupied levels. Under this assumption, we can estimate the probability distribution of the most weakly bound flux line by using the state at the chemical potential ψ_μ instead of $\psi_{\mathrm{g.s.}}$ in the above analysis.

III. DELOCALIZATION TRANSITION IN NON-HERMITIAN QUANTUM MECHANICS

We now sketch the mechanism of the delocalization in the non-Hermitian quantum system described above. Consider first localized states in a small transverse field $\mathbf{g}$. Assume that we know the eigenvalues ε_n and the eigenfunctions $\psi_n(\mathbf{x})$ for $\mathbf{g}=\mathbf{0}$. We can use the imaginary gauge transformation (2.22) to determine the eigenfunctions for small $\mathbf{g}$. The right eigenfunctions and the left eigenfunctions are given by

$$\psi_n^R(\mathbf{x};\mathbf{g}) = \mathcal{U} \psi_n(\mathbf{x};\mathbf{g}=\mathbf{0}), \tag{3.1}$$

$$\psi_n^L(\mathbf{x};\mathbf{g}) = \psi_n(\mathbf{x};\mathbf{g}=\mathbf{0}) \mathcal{U}^{-1}, \tag{3.2}$$

where

$$\mathcal{U} \equiv \exp\left(\frac{\mathbf{g} \cdot \mathbf{x}^{\mathrm{op}}}{\hbar} \right), \quad \mathcal{U}^{-1} \equiv \exp\left(-\frac{\mathbf{g} \cdot \mathbf{x}^{\mathrm{op}}}{\hbar} \right). \tag{3.3}$$

The corresponding energy eigenvalue ε_n is then unchanged provided that this imaginary gauge transformation is applicable. However, the above wave functions ψ_n^R and ψ_n^L may diverge as $|\mathbf{x}| \to \infty$ and become unnormalizable.[17] If we assume an asymptotic form of the wave function for $\mathbf{g}=\mathbf{0}$ of the form

$$\psi_n(\mathbf{x};\mathbf{g}=\mathbf{0}) \underset{x \to \infty}{\sim} \exp(-\kappa_n |\mathbf{x}-\mathbf{x}_n|), \tag{3.4}$$

the condition for nondivergence of ψ_n^R and ψ_n^L in $|\mathbf{x}| \to \infty$ is $|\mathbf{g}| < \hbar \kappa_n$. Then the normalized wave functions are approximately given by (see Fig. 5)

$$\psi_n^R \simeq \sqrt{\frac{(2\kappa_n)^d}{\Gamma(d)\Omega_d}} \exp[\mathbf{g} \cdot (\mathbf{x}-\mathbf{x}_n)/\hbar - \kappa_n |\mathbf{x}-\mathbf{x}_n|], \tag{3.5}$$

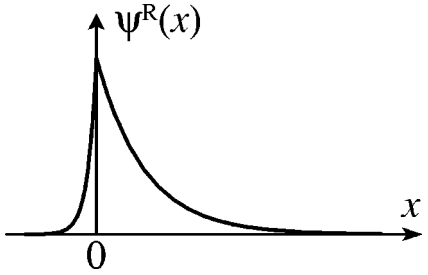

FIG. 5. Wave function (3.5) or (4.7), the ground state of a single impurity with $0<g<g_c$ in one dimension.

$$\psi_n^L \simeq \sqrt{\frac{(2\kappa_n)^d}{\Gamma(d)\Omega_d}}\exp[-\mathbf{g}\cdot(\mathbf{x}-\mathbf{x}_n)/\hbar-\kappa_n|\mathbf{x}-\mathbf{x}_n|], \tag{3.6}$$

where $\mathbf{x}_n$ is the localization center for $\mathbf{g}=\mathbf{0}$, Ω_d is the total solid angle of the d-dimensional space, and the normalization condition is

$$\int \psi_n^L \psi_n^R d^d\mathbf{x}=1. \tag{3.7}$$

We naturally regard the point $|\mathbf{g}|=\hbar\kappa_n$ as the delocalization point of the nth state. Since the eigenfunctions are proportional to the probability distribution of a flux line at the surfaces of the superconductor [see Eqs. (2.31) and (2.32)], we interpret the divergence in $|\mathbf{x}|\to\infty$ as depinning of the flux line. Because localized states with finite localization length are stable against a small $\mathbf{g}$ field, flux-line pinning is *robust* against small transverse field: This is the transverse Meissner effect.[10]

The diverging tilt slope in Eq. (1.10) follows because the localization length of the right eigenfunction is $(\kappa_n-|\mathbf{g}|/\hbar)^{-1}$ in the direction of $\mathbf{g}$ and $(\kappa_n+|\mathbf{g}|/\hbar)^{-1}$ in the opposite direction. The former diverges as $|\mathbf{g}|\to\hbar\kappa_n^-$; hence $H_{\perp c}=4\pi\hbar\kappa_n/\phi_0$ in Eq. (1.10). According to the relation (2.18), the surface displacement or ''localization length'' of the flux line is proportional to the surface transverse magnetization $M_{\perp s}$.

We need to specify boundary conditions in order to obtain a well-defined wave function in the thermodynamic limit. Consider for simplicity the periodic boundary conditions

$$\psi_n^R(L_x/2,y,\ldots)=\psi_n^R(-L_x/2,y,\ldots), \tag{3.8}$$

where we put the x axis parallel to $\mathbf{g}$. (The one-dimensional periodic system is realized in the setup shown in Fig. 4.) A wave function of the form (3.5) localized at the origin has a mismatch of the factor $\exp[-(\kappa_n-|\mathbf{g}|/\hbar)L_x]$ at the boundaries $x=\pm L_x/2$. This mismatch is exponentially small in the pinning regime $|\mathbf{g}|<\hbar\kappa_n$. Hence the wave functions (3.5) and (3.6) are excellent approximations when we take the thermodynamic limit, imposing the periodic boundary conditions (3.8).

In the depinning regime $|\mathbf{g}|\geqslant\hbar\kappa_n$, however, we need to change the wave functions drastically to meet the boundary conditions. To see what happens in this regime, consider the limit in which the random potential $V(\mathbf{x})$ may be neglected:

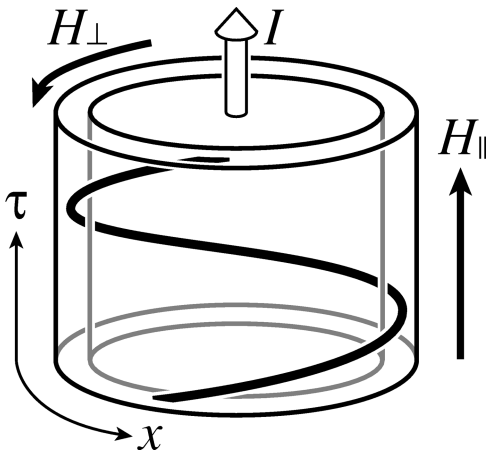

FIG. 6. Spiral trajectory of a flux line in the system of Fig. 4, reflecting the imaginary eigenvalues, which appear in non-Hermitian systems when boundary conditions allow nonzero tilt of vortex lines across the system.

$$\mathcal{H}_0=\frac{(\mathbf{p}+i\mathbf{g})^2}{2m}. \tag{3.9}$$

(We argue later that the potential in fact has only perturbative effects for large $\mathbf{g}$ when $d=1$.) The periodic boundary conditions (3.8) are then satisfied only by the extended Bloch wave

$$\psi^R(\mathbf{x})=\exp(i\mathbf{k}\cdot\mathbf{x}), \tag{3.10}$$

with $k_\nu=2n_\nu\pi/L_\nu$, where n_ν is an integer and L_ν is the system size in the x_ν direction. The eigenvalue of this wave function is complex:

$$\varepsilon(\mathbf{k})=\frac{(\hbar\mathbf{k}+i\mathbf{g})^2}{2m}. \tag{3.11}$$

We can interpret the appearance of the imaginary part of the energy in the following way. A depinned flux line in a periodic system has a spiral trajectory and hence periodicity in the imaginary time direction. (See Fig. 6.) Because the single-line partition function at ''time'' τ may be written $\mathcal{Z}(\tau)=\Sigma_n c_n\psi_n^R(\mathbf{x})e^{-\varepsilon_n\tau/\hbar}$, where the constants c_n are coefficients depending on ''initial conditions'' at, say, the bottom surface of the sample, the period of motion in the imaginary-time direction associated with the nth eigenstate is given by $\hbar/\mathrm{Im}\,\varepsilon_n$, where n denotes the wave function describing the depinned flux line. Thus a complex energy, as well as an imaginary part of the current (2.19), is an indicator of the depinning transition in periodic systems.

We use periodic boundary conditions in all directions perpendicular to the imaginary-time axis throughout this paper. The effect of ''free'' boundary conditions in the timelike direction is discussed in Sec. VII. For superconducting flux lines, unusual geometries such as Fig. 4 would be required to exactly implement periodic boundary conditions in the direction parallel to the tilt field $\mathbf{g}$. For conventional slablike superconducting samples, tilt causes extra vortices to enter and exit the sample on the sides perpendicular to $\mathbf{g}$. These bound-

ary conditions correspond to reservoirs and sinks of particles at opposite ends of the sample in the quantum analogy. Because periodic boundary conditions mimic the effects of such sources and sinks, we expect that the basic results of this paper apply to slablike geometries as well.

IV. ONE-DIMENSIONAL ONE-IMPURITY PROBLEM

In the present section we analyze the non-Hermitian Hamiltonian (1.1) analytically in one dimension with a single impurity. The calculation is instructive as well as of physical relevance for vortex lines in the case of a twin boundary. Throughout this section we assume without loss of generality that the non-Hermitian field is applied in the positive x direction, i.e., $g>0$.

A. Exact solution: Point impurity

To determine the effect of an isolated impurity, we calculate the right eigenvectors of the Schrödinger equation $\mathcal{H}\psi^R(x)=\varepsilon\psi^R(x)$ with the Hamiltonian defined by

$$\mathcal{H}\equiv\frac{(p+ig)^2}{2m}-V_0\delta(x)=-\frac{(\hbar\nabla-g)^2}{2m}-V_0\delta(x), \tag{4.1}$$

with $V_0>0$ and the periodic boundary conditions

$$\psi^R(L_x)=\psi^R(0). \tag{4.2}$$

The details of the solution are given in the Appendix. There is a unique localized ground state for $g<g_c$, where the critical field is

$$g_c\equiv\hbar\kappa_{\text{g.s.}}=\frac{mV_0}{\hbar}. \tag{4.3}$$

(Recall that the ground state is the state with the lowest *real* part of the eigenenergy.) This solution is the only localized state in the entire spectrum. There are extended excited states for $g<g_c$ as well as extended ground *and* excited states for $g>g_c$. For later use in Sec. IV B, we write down the solutions of the extended states including finite-size corrections.

First, the ground state for $g<g_c$ has the energy

$$\varepsilon_{\text{g.s.}}=-\frac{(\hbar\kappa_{\text{g.s.}})^2}{2m}=-\frac{mV_0^2}{2\hbar^2}, \tag{4.4}$$

with

$$\kappa_{\text{g.s.}}\equiv\frac{mV_0}{\hbar^2}. \tag{4.5}$$

Note that the ground-state energy is independent of g and equal, in particular, to the ground-state energy in the Hermitian case $g=0$. This observation is consistent with the pinning criterion given below Eq. (2.20). The current carried by the ground state therefore vanishes:

$$\text{Im}J_{\text{g.s.}}\equiv-\frac{\partial\varepsilon_{\text{g.s.}}}{\partial g}=0. \tag{4.6}$$

The corresponding eigenvector is a localized function written in the form

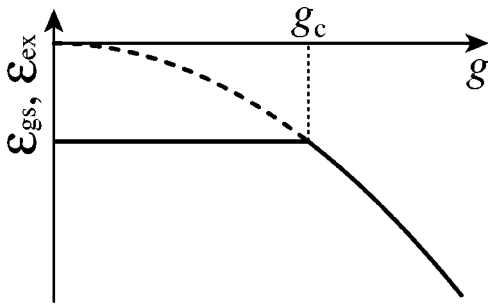

FIG. 7. g dependence of the ground-state energy (solid line) and the first-excited-state energy (dashed line) of the one-dimensional one-impurity problem.

$$\psi^R_{\text{g.s.}}(x)\propto\begin{cases}\exp[-(\kappa_{\text{g.s.}}-g/\hbar)x] & \text{for } x\geq 0\\ \exp[-(\kappa_{\text{g.s.}}+g/\hbar)|x|] & \text{for } x<0\end{cases} \tag{4.7}$$

in the limit $L_x\to\infty$. This is depicted in Fig. 5.

Next, the excited states for $g<g_c$ are given by

$$\varepsilon_{\text{ex}}=\frac{(\hbar K_{\text{ex}})^2}{2m}, \tag{4.8}$$

where

$$K_{\text{ex}}=k_{\text{ex}}+i\kappa_{\text{ex}}, \tag{4.9}$$

with

$$k_{\text{ex}}=\frac{(2n+1)\pi}{L_x}+O(L_x^{-2}), \tag{4.10}$$

$$\kappa_{\text{ex}}=\frac{g}{\hbar}+\frac{1}{L_x}\ln\frac{g}{g_c-g}+O(L_x^{-2}), \tag{4.11}$$

where n is an integer. The ground and excited states for $g>g_c$ are given by

$$\varepsilon_{\text{g.s.,ex}}=\frac{(\hbar K_{\text{g.s.,ex}})^2}{2m}, \tag{4.12}$$

where

$$K_{\text{g.s.,ex}}=k_{\text{g.s.,ex}}+i\kappa_{\text{g.s.,ex}}, \tag{4.13}$$

with

$$k_{\text{g.s.,ex}}=\frac{2n\pi}{L_x}+O(L_x^{-2}), \tag{4.14}$$

$$\kappa_{\text{g.s.,ex}}=\frac{g}{\hbar}+\frac{1}{L_x}\ln\frac{g}{g-g_c}+O(L_x^{-2}). \tag{4.15}$$

The case $n=0$ in Eq. (4.14) describes a delocalized ground state when $g>g_c$.

The leading term in the energy eigenvalues for the extended states (4.8) and (4.12) is

$$\lim_{L_x\to\infty}\varepsilon_{\text{g.s.,ex}}=-\frac{g^2}{2m}. \tag{4.16}$$

The energies of the ground state and the first excited state depend on g in the limit $L_x\to\infty$, as shown in Fig. 7. According to the pinning criterion given below Eq. (2.20), the ap-

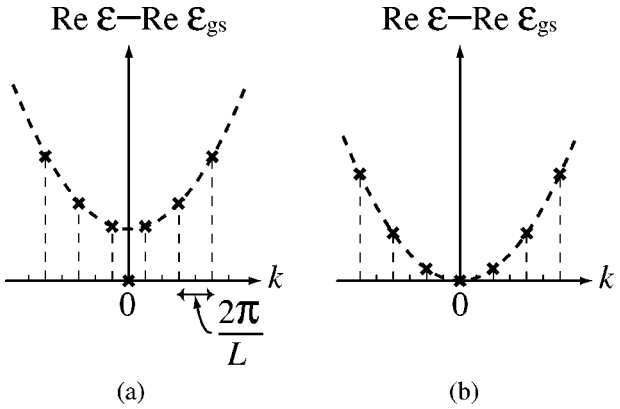

FIG. 8. Dispersion relation Reε vs k ($\propto$Imε) in the one-dimensional one-impurity case for (a) $g<g_c$ and (b) $g>g_c$.

pearance of the g dependence indicates that these are extended states. The current carried by each state is thus purely imaginary,

$$\lim_{L_x\to\infty} J_{\text{g.s.,ex}} = i\frac{g}{m}. \tag{4.17}$$

The eigenvectors corresponding to these extended states are

$$\psi^R_{\text{ex}}(x)\sim\begin{cases} e^{ik_{\text{ex}}x} & \text{for } x>0 \\ e^{ik_{\text{ex}}x}+ce^{-ik_{\text{ex}}x+2gx/\hbar} & \text{for } x<0 \end{cases} \tag{4.18}$$

in the limit $L_x\to\infty$, where c is a constant. The term $e^{ik_{\text{ex}}x}$ is a plane wave traveling in the x direction and the second term of the second line is the reflection due to the δ potential at the origin.

In Fig. 8 we plot the dispersion relation, that is, Reε against k ($\propto$Imε). Note the level repulsion between the impurity level and the extended states; as we increase g, the localized impurity level approaches the series of extended excited states and must squeeze itself into the sequence. Finally, the solutions at the critical point $g=g_c$ are again given by the form (4.12), but with

$$k_{\text{g.s.,ex}} = O(L_x^{-1}\ln L_x),$$

$$\kappa_{\text{g.s.,ex}} = \frac{g}{\hbar}+O(L_x^{-1}\ln L_x). \tag{4.19}$$

B. Flux-line depinning from a defect

We now apply the above solutions to flux-line physics in a thin cylindrical superconducting shell with one defect in it. The flux line undergoes a depinning transition when $g=g_c$. Its tilt slope, given as $L_\tau\to\infty$ by the imaginary current of the ground state, vanishes for $g<g_c$, but jumps to a finite value for $g>g_c$:

$$\text{Im}J_{\text{g.s.}} = \begin{cases} 0 & \text{for } g<g_c \\ g/m & \text{for } g>g_c. \end{cases} \tag{4.20}$$

This directly shows that the flux line is depinned from the defect at $g=g_c$. At this depinning point, the contribution of this flux line to the bulk transverse magnetization jumps by

$$\Delta M_\perp = \frac{\phi_0 g_c}{Am}, \tag{4.21}$$

where A is the cross-sectional area, because of the relations (2.18) and (2.20).

Although the above jump appears to indicate a first-order transition,[14] we shall argue in Sec. VIII that the bulk magnetization in fact grows continuously at the transition when interactions are taken into account. There are, moreover, diverging precursors of the destruction of the transverse Meissner effect as $g\to g_c^-$. As discussed in Sec. II C, the normalized right eigenvector gives the probability distribution of the corresponding flux line at the top surface. The wave function (4.7) in the pinning regime ($g<g_c$) defines a surface localization length $\xi_\perp$ of the flux line as $\xi_\perp\equiv(\kappa_{\text{g.s.}}-g/\hbar)^{-1}$, which diverges as $g\to g_c^-$,

$$\xi_\perp\sim\frac{\hbar}{g_c-g}. \tag{4.22}$$

The transverse magnetization near the surface diverges like $\xi_\perp$,

$$M_{\perp s}\propto\langle x\rangle_{L_\tau}-\langle x\rangle_{L_\tau/2} = \frac{(\kappa_{\text{g.s.}}-g/\hbar)^{-2}+(\kappa_{\text{g.s.}}+g/\hbar)^{-2}}{(\kappa_{\text{g.s.}}-g/\hbar)^{-1}+(\kappa_{\text{g.s.}}+g/\hbar)^{-1}} \tag{4.23}$$

$$\simeq\frac{\hbar}{g_c-g} \tag{4.24}$$

(in the limit $L_\tau,L_x\to\infty$) as the vortex line begins to tear free.

We show below that the displacement of the flux line from the defect depends on the depth from the surface according to

$$\langle x\rangle_\tau\sim\exp\left(-\frac{\tau}{\tau^*}\right) \tag{4.25}$$

as $\tau\to\infty$, where τ denotes the distance below the surface. (See Sec. VII for the many-defect case.) The penetration depth τ^* diverges at the depinning point $g=g_c$ as

$$\tau^*\simeq\frac{m\hbar/g_c}{g_c-g}\quad\text{as } g\to g_c^-. \tag{4.26}$$

The exponent of the penetration-depth divergence is the same as the one of the surface-localization-length divergence (4.22): If we define the exponent z by $\tau^*\sim(\xi_\perp)^z$, we have $z=1$. (The exponent is different in the many-defect case; see Sec. VII.)

The divergence (4.26) is derived as follows: Expand Eq. (2.13) with respect to eigenfunctions and take the limit $L_\tau\to\infty$ in Eq. (2.13) to obtain

$$\langle x\rangle_\tau\simeq\sum_n c_n\int dx\langle\psi_{\text{g.s.}}|x\rangle x\langle x|\psi_n\rangle e^{-\tau\Delta\varepsilon_n/\hbar}, \tag{4.27}$$

where

$$c_n\equiv\frac{\int\langle\psi_n|x'\rangle dx'}{\int\langle\psi_{\text{g.s.}}|x'\rangle dx'} \tag{4.28}$$

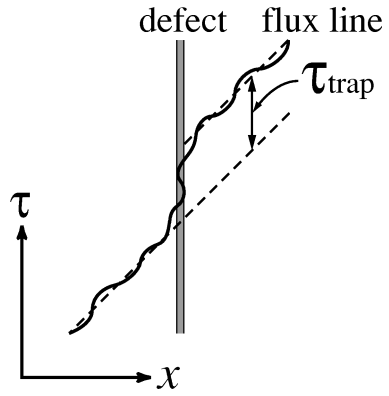

FIG. 9. Definition of the trapping length $\tau_{\rm trap}$.

and

$$\Delta\varepsilon_n \equiv \varepsilon_n - \varepsilon_{\rm g.s.}. \tag{4.29}$$

The term $\psi_n = \psi_{\rm g.s.}$ in the summation over n gives the position of the localization center of the ground state, namely, the origin. Hence the leading term is due to the first excited state. Then the penetration depth τ^* in Eq. (4.25) is given by the inverse energy gap between the ground state and the first excited state,

$$\tau^* \equiv \frac{\hbar}{\Delta\varepsilon} = \frac{2m\hbar}{g_c^2 - g^2}, \tag{4.30}$$

which leads to Eq. (4.26).

There are also diverging precursors on the other side of the transition ($g \to g_c^+$) in the form of a diverging finite-size correction, namely, the trapping length. The trapping length is defined as follows (see Fig. 9). The average slope of the flux line for $x \neq 0$ should be given by the tilt slope of a flux line in the absence of defects, or g/m. Assume that the flux line is trapped by the defect at $x = 0$ over the distance $\tau_{\rm trap}$. Then the total imaginary time necessary for a flux line to circle the periodic system of circumference L_x is $L_x m/g + \tau_{\rm trap}$. Thus the mean tilt slope (or the imaginary part of the current) should be given by $\mathrm{Im}J_{\rm g.s.} = L_x (L_x m/g + \tau_{\rm trap})^{-1}$. This in turn gives the definition of the trapping length as

$$\tau_{\rm trap} \equiv L_x \left(\frac{1}{\mathrm{Im}J_{\rm g.s.}} - \frac{m}{g} \right). \tag{4.31}$$

For this to be finite in the limit $L_x \to \infty$, the imaginary part of the current should have a finite-size correction of the form

$$\mathrm{Im}J_{\rm g.s.} \simeq \frac{g}{m} \left(1 - \frac{\tau_{\rm trap} g/m}{L_x} \right). \tag{4.32}$$

In fact, the correction (4.15) has precisely this form:

$$\mathrm{Im}J_{\rm g.s.} = \frac{\partial}{\partial g} \frac{\hbar^2 [\kappa_{\rm g.s.}(\infty) + \delta\kappa_{\rm g.s.}(L_x)]}{2m}$$
$$\simeq \frac{g}{m} \left(1 + \frac{\hbar\,\delta\kappa_{\rm g.s.}}{g} + \hbar \frac{\partial \delta\kappa_{\rm g.s.}}{\partial g} \right). \tag{4.33}$$

We thereby obtain

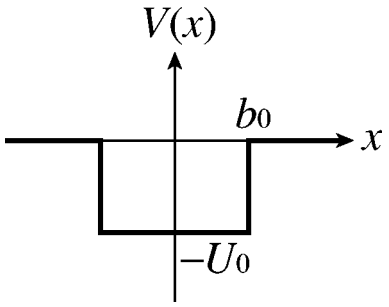

FIG. 10. Square-well impurity potential treated in Sec. IV C.

$$\tau_{\rm trap} = \frac{m\hbar}{g^2} \left(\frac{g_c}{g - g_c} - \ln \frac{g}{g - g_c} \right) \simeq \frac{m\hbar/g_c}{g - g_c}, \tag{4.34}$$

which has a simple pole as we approach the pinning point $g = g_c$ from the depinning regime.

C. Exact solution: Square-well potential

We can also solve the one-dimensional problem exactly for a single square-well impurity as shown in Fig. 10. We here restrict ourselves to localized states. The equation (A12) for the δ-potential case is now replaced by

$$2k\kappa\{\cosh(L_x g/\hbar) - \cos(2kb_0)\cosh[\kappa(L_x - 2b_0)]\}$$
$$+ (k^2 - \kappa^2)\sin(2kb_0)\sinh[\kappa(L_x - 2b_0)] = 0, \tag{4.35}$$

where

$$k \equiv \frac{\sqrt{2m(U_0 - |\varepsilon|)}}{\hbar}, \quad \kappa \equiv \frac{\sqrt{2m|\varepsilon|}}{\hbar}. \tag{4.36}$$

The equation for the δ potential is recovered in the limit $b_0 \to 0$ and $U_0 \to \infty$ with $2b_0 U_0 = V_0$.

The results are quite similar to the δ-potential case. The critical field of the delocalization transition is again given by

$$g_c = \lim_{L_x \to \infty} \hbar\kappa(L_x), \tag{4.37}$$

where $\kappa(L_x)$ is a solution of Eq. (4.35) with $g = 0$. In the limit $L_x \to \infty$ with $g = 0$, Eq. (4.35) is reduced to

$$2k\kappa\,\cos(2kb_0) + (\kappa^2 - k^2)\sin(2kb_0) = 0 \tag{4.38}$$

or

$$[\kappa\,\sin(kb_0) + k\,\cos(kb_0)][\kappa\,\cos(kb_0) - k\,\sin(kb_0)] = 0. \tag{4.39}$$

Upon setting $\overline{\kappa} \equiv b_0\kappa$ and $\eta \equiv b_0 k$, we are led to

$$\overline{\kappa}^2 + \eta^2 = \alpha^{-2} \tag{4.40}$$

and

$$\overline{\kappa} = \eta\,\tan\,\eta \quad \text{or} \quad \overline{\kappa} = -\eta\,\cot\,\eta, \tag{4.41}$$

where

$$\alpha \equiv \frac{\hbar}{b_0\sqrt{mU_0}} \tag{4.42}$$

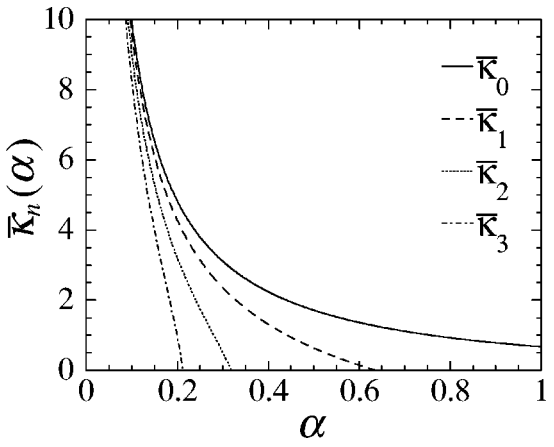

FIG. 11. Solution $\overline{\kappa_n}(\alpha)$ of Eqs. (4.40) and (4.41), which is proportional to the depinning field $H_{\perp c}$ of a single square-well impurity. The ground-state function $\overline{\kappa_0}(\alpha)$ and the first three excited states are shown.

is the ''reduced temperature''[10] in the sense that $\hbar$ corresponds to the temperature of the flux-line system. There is always at least one solution of Eqs. (4.40) and (4.41), including the ground state. More localized excited states are available for small α, which corresponds to the low temperature of the flux-line system. Each state is localized for $g<g_c=\hbar\kappa(\infty)$, where κ is the inverse localization length of the state at $g=0$. Figure 11 shows the α dependence of $\overline{\kappa_n}(\alpha)$ for the ground state and the first few excited states. The depinning transverse field for the nth state is $H_{\perp c}=(4e/cb_0)\overline{\kappa_n}(\alpha)$ for the ground state as well as for the excited states. The divergences discussed in Sec. IV B for the δ-function potential problem also apply to the present case.

V. ONE-DIMENSIONAL RANDOM NON-HERMITIAN TIGHT-BINDING MODEL

In this section we present numerical results for a one-dimensional random system. To make the numerical calculation tractable, we use lattice non-Hermitian random tight-binding models (1.2), where the sites represent column positions with random binding energies and/or hopping matrix elements, as in Fig. 4.

A. Site-random model

First we discuss the site-random model. The second-quantized Hamiltonian in d dimensions is given by Eq. (1.2). (Boson notation is used here because flux lines behave like bosons in the delocalized regime, although statistics are irrelevant when the lines are strongly localized.) The hopping element is approximately[10]

$$t\sim V_{\rm bind}\exp(-\sqrt{2mV_{\rm bind}}a/\hbar), \tag{5.1}$$

where $V_{\rm bind}$ is a typical binding energy of the defect and a is the lattice spacing. We again apply periodic boundary conditions

$$b_{\mathbf{x}+N_\nu\mathbf{e}_\nu}=b_{\mathbf{x}}\quad\text{for}\quad\nu=1,2,\ldots,d, \tag{5.2}$$

where $N_\nu\equiv L_\nu/a$.

The issues involved in determining the spectrum of Eq. (1.2) are especially easy to illustrate in one dimension. In an N-site basis with lattice spacing a, $\mathcal{H}$ takes an approximately tridiagonal form

$$\mathcal{H}=-\frac{1}{2}t\begin{pmatrix} v_1 & e^{\overline{g}} & & & & & e^{-\overline{g}} \\ e^{-\overline{g}} & v_2 & e^{\overline{g}} & & & 0 & \\ & e^{-\overline{g}} & v_3 & e^{\overline{g}} & & & \\ & & e^{-\overline{g}} & v_4 & \ddots & & \\ & & & \ddots & \ddots & \ddots & \\ & 0 & & & \ddots & v_{N-1} & e^{\overline{g}} \\ e^{\overline{g}} & & & & & e^{-\overline{g}} & v_N \end{pmatrix}, \tag{5.3}$$

with $v_n\equiv -2V_n/t$ and $\overline{g}\equiv ga_0/\hbar$. Delocalization of the eigenfunctions is traditionally associated with an extreme sensitivity to boundary conditions;[20,21] the periodic boundary conditions used here are reflected in the nonzero matrix elements in the upper right and lower left corners. For the present non-Hermitian problem, delocalization is reflected in an extreme sensitivity of the *eigenvalues*. Suppose the (real) eigenvalue spectrum is known exactly for the Hermitian site-random problem with $\overline{g}=0$. One expects all states to be localized for this one-dimensional problem. If the entries in the upper right and lower left corners are arbitrarily set to zero, it is easily shown that *all* eigenvalues for general $\overline{g}$ remain real and strictly equal to their values for $\overline{g}=0$. As will be shown in this section, the eigenvalue spectrum for the original periodic problem becomes complex in the middle of the band for $\overline{g}$ above a threshold value of $\overline{g}_c>0$. These complex eigenvalues are thus entirely due to the presence of nonzero upper right and lower left matrix elements. For this non-Hermitian random problem, complex eigenvalues therefore indicate directly the extreme sensitivity to boundary conditions associated with delocalized states.

For columnar defects, an important component of the randomness often comes from position of the extended defects rather than on-site disorder as assumed in this tight-binding model. However, if we coarse grain a system with the positional randomness, the resulting effective Hamiltonian will contain on-site disorder.[10] By varying the energy and type of heavy ions that produce columnar defects, one can also generate on-site disorder directly. We expect that similar energy spectra and delocalization phenomena arise for both random-site and random-hopping models and will present results for a random hopping model in Sec. V C.

Similar to the discussion below Eq. (2.16) for the continuum model, the eigenvalues of the non-Hermitian lattice model (1.2) also appear in complex conjugate pairs, thus ensuring that the partition function $\mathcal{Z}$ is real. Another symmetry is

$$\mathcal{H}(\mathbf{g})^T=\mathcal{H}(-\mathbf{g}). \tag{5.4}$$

Because of this symmetry, the right eigenfunction of $\mathcal{H}(\mathbf{g})$ is equal to the left eigenfunction of $\mathcal{H}(-\mathbf{g})$ with the same eigenvalue.

If $V_{\mathbf{x}}\equiv 0$, eigenstates are Bloch waves and the eigenvalues for general dimension d are

$$\varepsilon(\mathbf{k}) = -t\sum_{\nu=1}^{d} \cos[(k_\nu + ig_\nu/\hbar)a] \tag{5.5}$$

or

$$\mathrm{Re}\varepsilon(\mathbf{k}) = -t\sum_{\nu=1}^{d} \cos(k_\nu a)\cosh(g_\nu a/\hbar),$$

$$\mathrm{Im}\varepsilon(\mathbf{k}) = t\sum_{\nu=1}^{d} \sin(k_\nu a)\sinh(g_\nu a/\hbar), \tag{5.6}$$

with $k_\nu = 2n_\nu\pi/L_\nu$, where n_ν is an integer. In one dimension, the eigenvalues lie on an ellipse, given by

$$\left[\frac{\mathrm{Re}\varepsilon}{\cosh(ga/\hbar)}\right]^2 + \left[\frac{\mathrm{Im}\varepsilon}{\sinh(ga/\hbar)}\right]^2 = t^2. \tag{5.7}$$

Its low-energy structure is the same as the dispersion relation (3.11) of the impurity-free continuum model (3.9). The high end of the ellipse (5.7) is the dispersion relation for hole excitations. The eigenfunctions take the form $\psi^R(\mathbf{x}) \propto \exp(i\mathbf{k}\cdot\mathbf{x})$, with $\psi^L(\mathbf{x}) \propto \exp(-i\mathbf{k}\cdot\mathbf{x})$.

Numerical calculations for $V_\mathbf{x} \neq 0$ were carried out with a random potential $V_\mathbf{x}$ uncorrelated in space and uniformly distributed in the range $[-\Delta, \Delta]$. For such a symmetric distribution, the complex spectrum is statistically symmetric with respect to the axis $\mathrm{Re}\varepsilon = 0$.

Figure 12(a) shows the $d=1$ spectrum with $N=1000$ sites for various values of $\bar{g}$. As discussed above, a complex eigenvalue indicates that a flux line occupying that state is depinned. There is a region of $\bar{g}$ where all the eigenstates are localized. As we increase $\bar{g}$ further, the first delocalized state appears in the band center and a pair of mobility edges move outward toward the band edges. As long as an eigenvalue is real or the eigenstate is localized, the eigenvalue is independent of $\bar{g}$; see Fig. 12(b) for an expanded version of the bottom of the band: The localized eigenvalues are in perfect registry for different values of $\bar{g}$. The behavior of the delocalized states, on the other hand, is similar to the impurity-free case (5.7) except near the mobility edges. Close to the mobility edge the imaginary part of the eigenvalue appears to vanish *linearly* with the real part of the eigenvalue.

In Fig. 13 we show the imaginary part of the current defined by Eq. (2.16), another indicator of the delocalization transition. Upon comparing Fig. 13 with Fig. 12(a), we note that, for each value of $\bar{g}$, the states with complex eigenvalues coincide with those carrying a nonzero imaginary current. This observation is consistent with the mechanism of the delocalization transition presented in Sec. III. The negative imaginary part of the current in the upper half of the band is due to delocalization of hole excitations.

States near the band center get delocalized first because the inverse localization lengths κ are smaller near the band center than near the band edges. Figure 14 shows the result of a numerical calculation of an approximate inverse localization length for $\bar{g}=0$, defined by

$$\kappa_n' \equiv \left\langle \sqrt{\int x^2|\psi_n(x)|^2dx - \left(\int x|\psi_n(x)|^2\right)^2} \right\rangle_{\mathrm{av}}, \tag{5.8}$$

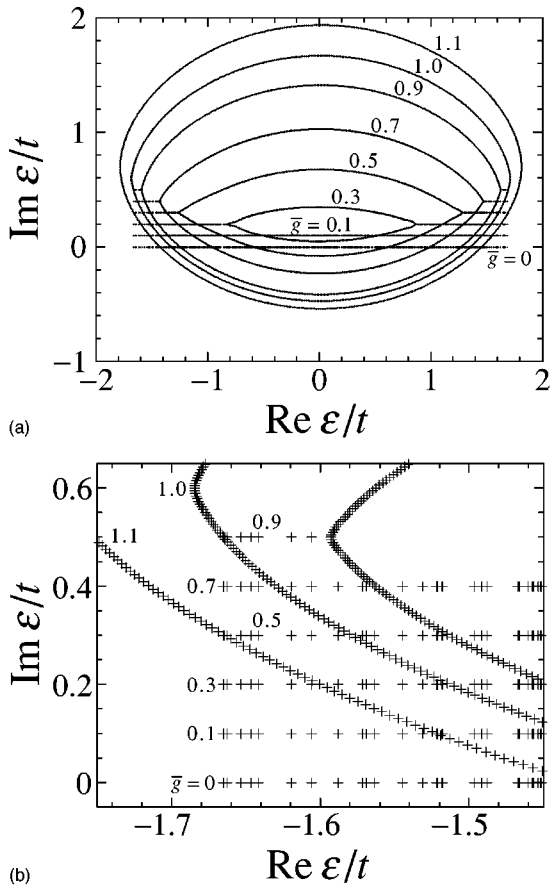

FIG. 12. (a) Energy spectrum of the one-dimensional tight-binding model with randomness $\Delta/t=1$ and $L_x=1000a$. Plots for different values of $\bar{g}\equiv ga/\hbar$ are offset for clarity. The same realization of the random potential was used for all plots here. Each eigenstate is marked by a cross. (b) Blowup of a part of (a); note that the real eigenvalues, corresponding to localized states, are independent of $\bar{g}$.

where we took the random average $\langle\ \rangle_{\mathrm{av}}$ over 100 realizations of the random potential. According to the delocalization criterion $g_c = \hbar\kappa$, delocalized states appear first at the band center and the mobility edges move outward, in agreement with our numerical results.

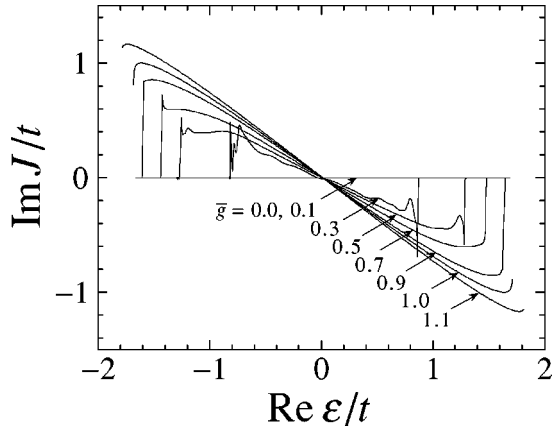

FIG. 13. Imaginary part of the current (or the tilt slope of the corresponding flux line) plotted against $\mathrm{Re}\varepsilon$ for the same sample as in Fig. 12.

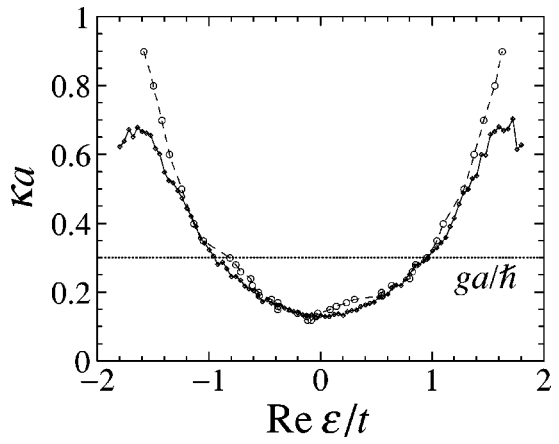

FIG. 14. The solid curve shows an approximate inverse localization length κ', as determined from Eq. (5.8), plotted against Reε for $\Delta/t=1$, $L_x=500a$, and $g=0$. The value was averaged over 100 samples binned with energy window $0.04t$. The dashed line shows an estimation of κ based on the delocalization criterion $g_c=\hbar\kappa$. For this purpose, we applied increasing g to a sample of size $L_x=500a$. The states at the mobility edges for a value of g (e.g., the dotted line) have the inverse localization length $\kappa=g/\hbar$.

In practice, it is convenient to *define* the inverse localization length using the delocalization criterion $g_c=\hbar\kappa$ (Ref. 17) instead of using Eq. (5.8); if a state becomes delocalized at a certain value g_c, the inverse localization length of the state is then $\kappa=g_c/\hbar$, shown as a dashed line in Fig. 14. The numerical estimation of κ using Eq. (5.8) is difficult near the band edges, where the number of data points is small, and hence a large statistical error appears. In addition, the definition (5.8) is not tied directly to the asymptotic behavior $\exp(-\kappa|x-x_n|)$.

B. Probability distribution of a flux line

Diagonalization of the lattice Hamiltonian (1.2) enables us to calculate the imaginary-time evolution of the wave function and more importantly the probability distribution of the flux line, Eq. (2.27). The expansion of Eq. (2.27) with respect to the energy eigenstates results in

$$P(\mathbf{x};\tau)=\frac{1}{\mathcal{Z}}\sum_{m,n}\langle\psi^f|\psi_m\rangle\langle\psi_m|\mathbf{x}\rangle\langle\mathbf{x}|\psi_n\rangle \times\langle\psi_n|\psi^i\rangle e^{-(L_\tau-\tau)\varepsilon_m/\hbar-\tau\varepsilon_n/\hbar}, \tag{5.9}$$

with

$$\mathcal{Z}=\sum_n e^{-L_\tau\varepsilon_n/\hbar}\langle\psi^f|\psi_n\rangle\langle\psi_n|\psi^i\rangle. \tag{5.10}$$

In the limit $L_\tau\to\infty$, in particular, we have

$$P(\mathbf{x};\tau)\simeq\frac{\langle\psi_{\text{g.s.}}|\mathbf{x}\rangle}{\langle\psi_{\text{g.s.}}|\psi^i\rangle}\sum_n\langle\mathbf{x}|\psi_n\rangle\langle\psi_n|\psi^i\rangle e^{-\tau\Delta\varepsilon_n/\hbar}, \tag{5.11}$$

where $\Delta\varepsilon_n\equiv\varepsilon_n-\varepsilon_{\text{g.s.}}$.

We used this formula to demonstrate numerically, for a particular realization of the random potential, that a flux line in the one-dimensional random system tips over near the surface under the influence of the transverse magnetic field. For $g=g_c$, the flux line is strictly localized for large τ at the strongest pinning center. As we increase g, kink configurations arise that allow hopping from one pin to the next. Figure 15(a) shows $P(\mathbf{x};\tau)$ for ''free'' boundary conditions at the bottom ($\tau=0$) of the sample, corresponding to

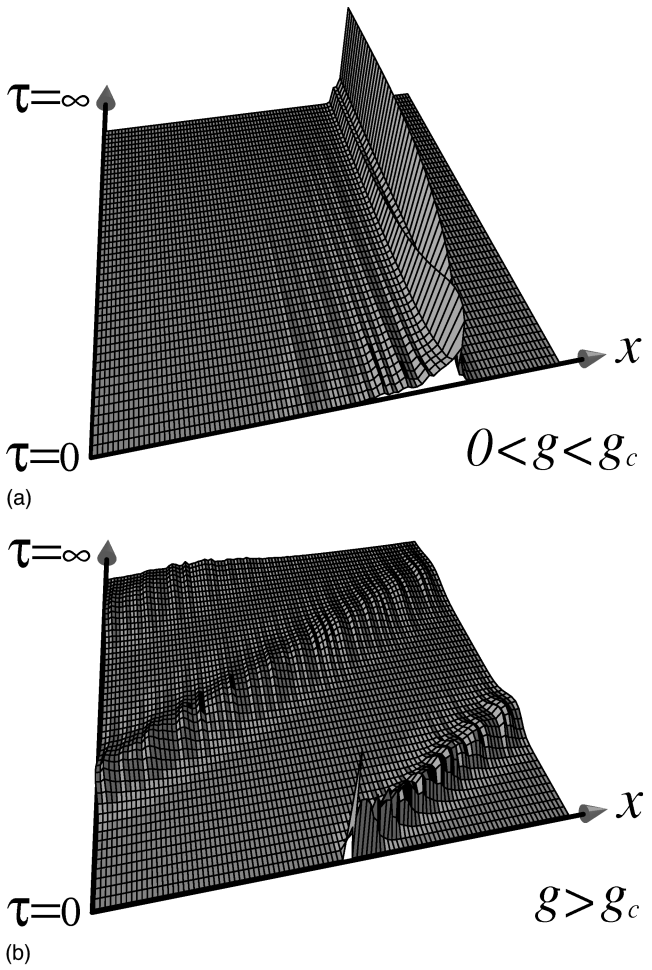

FIG. 15. Probability distribution of a flux line as a function of τ for the one-dimensional random tight-binding model (1.2) with a specific random potential $V(x)$ with $\Delta/t=1$. The spatial size is $L_x=100a$. The front end of the figures corresponds to the bottom surface of the superconductor, while the bulk part $\tau>50\hbar/t$ is omitted. (a) Case $\overline{g}=0.8<\overline{g_c}$ with free boundary conditions and (b) case $\overline{g}=2.0>\overline{g_c}$ with a δ-function initial condition. [The peak at $\tau=0$ in (b) has been reduced in size for visualization purposes.]

$$|\psi^i\rangle\equiv\int d\mathbf{x}|\mathbf{x}\rangle. \tag{5.12}$$

Note that the probability distribution near the surface has been pulled in the negative x direction by the transverse field. Once the flux line is depinned, spiral trajectories arise. To see this more clearly, we show in Fig. 15(b) the probability distribution for large g with the initial vector

$$|\tilde{\psi}^i\rangle\equiv|\mathbf{x}_0\rangle, \tag{5.13}$$

so that the end of the flux line is fixed to x_0 for $\tau=0$.

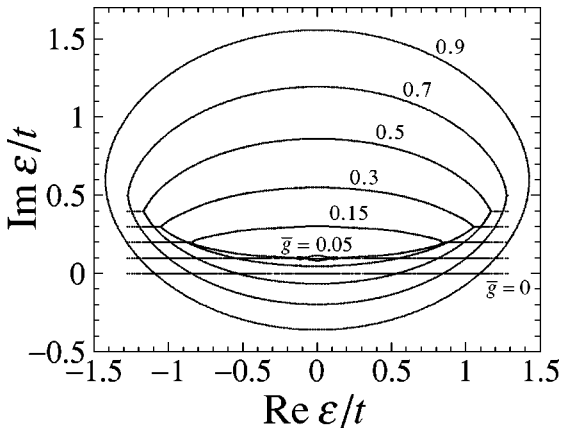

FIG. 16. Energy spectrum of the random-hopping model (5.14) with the randomness defined by Eqs. (5.15) and (5.16). The parameter values are $L=1000\overline{a}$ and $\Delta/t_0=0.5$.

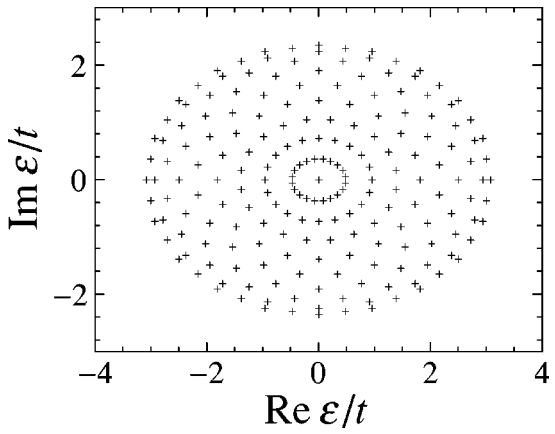

FIG. 17. Energy spectrum of the two-dimensional non-Hermitian tight-binding model without impurities, with $g_x=g_y=1.0\times\hbar/a$ and $L_x=L_y=20a$.

C. Random-hopping model

A one-dimensional Hamiltonian with off-diagonal randomness may be more suitable for describing the experimental situation in Ref. 16 than the present diagonal randomness. Mutually parallel twin boundaries might represent the pinning potential in this situation. As discussed above, we project out the coordinate that is parallel to the twin boundaries and perpendicular to the τ axis. Randomness arises from the separation of the binding twin boundaries rather than from the strength of the pinning. Thus we have

$$\mathcal{H}\equiv-\frac{1}{2}\sum_j\ (t_j^{+}b_{j+1}^{\dagger}b_j+t_j^{-}b_j^{\dagger}b_{j+1}), \tag{5.14}$$

where $t_j^{\pm}\equiv V_{\rm bind}\exp[(-\lambda\pm g)a_j/\hbar]$, $\lambda\equiv\sqrt{2mV_{\rm bind}}$, and a_j is the separation between the jth and $(j+1)$th binding impurities. If the twin boundaries are located randomly, the random separation follows the Poisson distribution $P(a_j)=\overline{a}^{-1}e^{-a_j/\overline{a}}$, where $\overline{a}$ is the average separation.

The delocalization phenomenon discussed above arises in this off-diagonal case as well; see Fig. 16. In this example we neglect the randomness embodied in the factor $\exp[\pm ga_j/\hbar]$ and use a square distribution of the hopping elements

$$t^{\pm}\equiv te^{\pm g\overline{a}/\hbar}, \tag{5.15}$$

where t is a random variable with probability

$$P(t)=\begin{cases}1/(2\Delta) & \text{for } t_0-\Delta<t<t_0+\Delta\ (t_0>\Delta)\\ 0 & \text{otherwise.}\end{cases} \tag{5.16}$$

Figure 16 is remarkably similar to the one-dimensional spectrum found earlier for site randomness.[22] The currents carried by the extended states resemble those shown in Fig. 13.

VI. TWO-DIMENSIONAL NON-HERMITIAN TIGHT-BINDING MODEL

We now discuss numerical results for the tight-binding model (1.2) in two dimensions for a square lattice with $L_x=L_y$. We assume $g_x=g_y$, i.e., a tilt field along the diagonal, in order to reduce artifacts due to lattice periodicity.

A. Impurity-free case and one-impurity case

First we describe the impurity-free case of the non-Hermitian tight-binding model (1.2):

$$V_{\mathbf{x}}\equiv 0. \tag{6.1}$$

The energy eigenvalues are given by Eq. (5.6) with $d=2$. In the case of $g_x=g_y\equiv g$, we have

$$\begin{aligned}\mathrm{Re}\varepsilon&=-2t\,\cosh\left(\frac{ga}{\hbar}\right)\cos\frac{(k_x+k_y)a}{2}\cos\frac{(k_x-k_y)a}{2},\\ \mathrm{Im}\varepsilon&=2t\,\sinh\left(\frac{ga}{\hbar}\right)\sin\frac{(k_x+k_y)a}{2}\cos\frac{(k_x-k_y)a}{2},\end{aligned} \tag{6.2}$$

with

$$\begin{aligned}k_x&=0,\pm\frac{2\pi}{L_x},\pm\frac{4\pi}{L_x},\ldots,\\ k_y&=0,\pm\frac{2\pi}{L_y},\pm\frac{4\pi}{L_y},\ldots,\end{aligned} \tag{6.3}$$

or

$$\left[\frac{\mathrm{Re}\varepsilon}{\cosh(ga/\hbar)}\right]^2+\left[\frac{\mathrm{Im}\varepsilon}{\sinh(ga/\hbar)}\right]^2=4t^2\,\cos^2\left(\frac{k_x-k_y}{2}a\right). \tag{6.4}$$

Thus the spectrum consists of ellipses with various radii as is shown for $N_x=N_y\equiv N=20$ in Fig. 17. Two levels with k_x and k_y interchanged are degenerate at each cross of the figure except for the point $\varepsilon=0$, where N levels with $k_x-k_y=\pi/a$ (mod $2\pi/a$) are degenerate. The eigenfunctions have the usual Bloch form

$$|\mathbf{k}\rangle\equiv b_{\mathbf{k}}^{\dagger}|0\rangle\equiv\frac{1}{\sqrt{L_xL_y}}\sum_{\mathbf{x}}\ e^{i\mathbf{k}\cdot\mathbf{x}}b_{\mathbf{x}}^{\dagger}|0\rangle. \tag{6.5}$$

The important phenomenon of level repulsion in the complex plane can be illustrated with one attractive point impurity

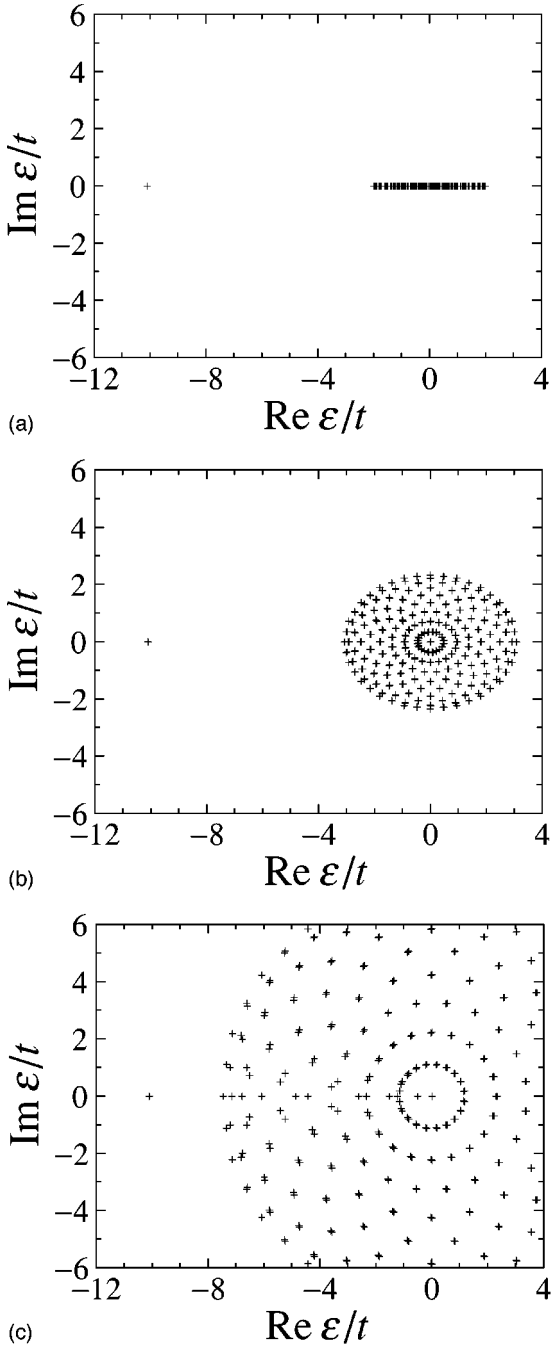

FIG. 18. Energy spectra of the two-dimensional non-Hermitian tight-binding model with one attractive impurity of well depth U_0. We show here the case $L_x=L_y=20a$ and $U_0=10t$ with (a) $g_x=g_y=0$, (b) $g_x=g_y=1.0\times\hbar/a$, and (c) $g_x=g_y=2\times\hbar/a$.

$$V_{\mathbf{x}}=-U_0\delta_{\mathbf{x}\mathbf{x}_0}, \tag{6.6}$$

where $\mathbf{x}_0$ denotes the position of the impurity. Figure 18 shows the results for the 20×20 lattice with periodic boundary conditions. Without the transverse field, we have one impurity level separated from a cluster of (delocalized) excited states, as seen in Fig. 18(a). As we introduce $\mathbf{g}$ diagonally ($g_x=g_y$), most excited states acquire imaginary eigenvalues [Fig. 18(b)], showing a spectrum similar to the impurity-free case, Fig. 17. The localized impurity level does not change its energy as long as $|\mathbf{g}|<g_c$, while the extended excited levels expand, following Eq. (6.4) of the impurity-free case approximately. In Fig. 18(c) we observe level repulsion between the impurity level and the excited levels. Note that the twofold degeneracy of the pure system is split on the side of the spectrum, where the impurity state is about to enter. For even larger $|\mathbf{g}|$, the bound state enters the region of delocalized levels and the spectrum is again elliptical with an extra state near the origin.

B. Random case

In the two-dimensional random tight-binding model, we again find energy bands of localized levels bounded by a mobility edge. For certain values of $\mathbf{g}$, however, extended and localized states are *mixed* in a complicated way near the band center. It appears that we have three regimes with respect to the field $\mathbf{g}$. One is the pinning phase for small $\mathbf{g}$. Another is the Bloch-wave regime for large $\mathbf{g}$. Finally, there is an exotic intermediate regime with chaotic eigenvalue spectra. We describe these regimes on the basis of our numerical data.

First, it is widely accepted for $\mathbf{g}=\mathbf{0}$ that all eigenstates of two-dimensional random systems are localized with finite localization lengths (except for a possible exception at the band center[22]). Hence there is again a region of small $\mathbf{g}$ where all states remain localized. As discussed earlier, these localized states retain the real eigenvalues that they had for $\mathbf{g}=\mathbf{0}$; see the energy spectrum in Fig. 19(a) for an example with $N_x=N_y=40$.

As we increase $\mathbf{g}$, delocalized levels with complex eigenvalues appear as shown in the energy spectrum in Fig. 19(b). A remarkable difference of the energy spectrum from the one-dimensional case is that localized levels and delocalized levels coexist in the same range of $\mathrm{Re}\varepsilon$ in the two-dimensional case. This phenomenon can be understood in terms of *anisotropic* localization of the Hermitian system (in the case $\mathbf{g}=\mathbf{0}$). To take advantage of anisotropic fluctuations in the site potential, there can be states with different localization lengths in specific directions. As shown schematically in Fig. 20, in a large system there can be another state with nearly the same energy, but whose contours are rotated by 90° from the first one. According to the argument developed in Sec. III, the delocalization point of each state is $g_c=\hbar\kappa$, where κ is now the inverse localization length of the state in the direction of $\mathbf{g}$. The state with the largest localization length in the direction of $\mathbf{g}$ gets delocalized first. Up to the delocalization point, however, both states have nearly identical real energies.

After passing through an intermediate region whose energy spectrum is exemplified in Fig. 19(c), we move onto the region of large $\mathbf{g}$. The energy-spectrum structure shown in Fig. 19(d) is similar to the impurity-free case shown in Fig. 17.

It is tempting to conclude from Fig. 19(d) that the large-$\mathbf{g}$ limit is well described by the extended Bloch-wave functions, just as in one dimension. However, unlike $d=1$, the Bloch approximation breaks down in $d=2$ for sufficiently large systems for *any* value of $\mathbf{g}$. To see this, recall that all Bloch states $|k_x,k_y\rangle$ with $k_x\neq k_y$ are twofold degenerate in the impurity-free case: If $\mathbf{g}$ points along the lattice diagonal as in Eq. (6.2), then $|k_x,k_y\rangle$ and $|k_y,k_x\rangle$ have the same com-

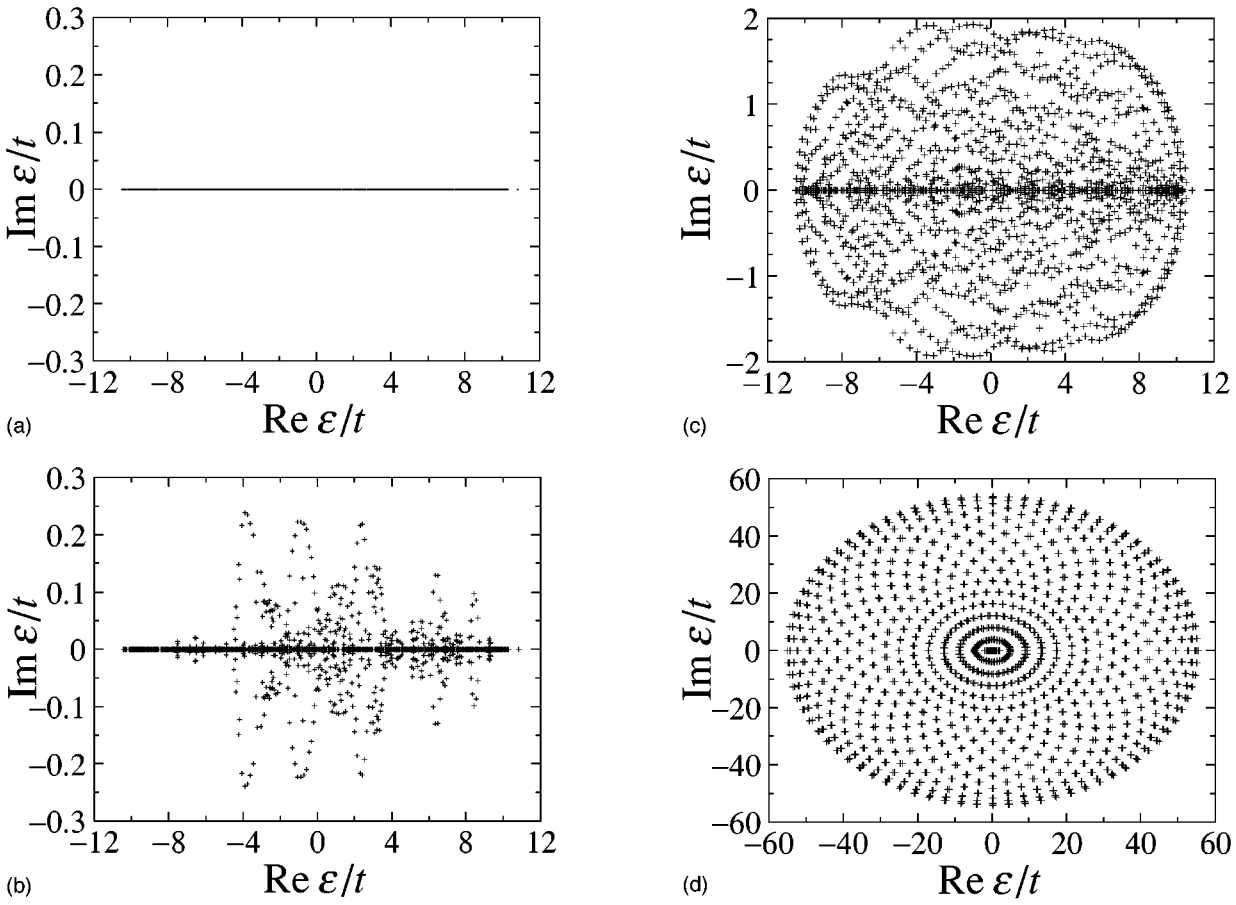

FIG. 19. Energy spectra of the two-dimensional non-Hermitian tight-binding model with site randomness. We show here the case $L_x=L_y=40a$ and $\Delta=10t$ with (a) $g_x=g_y=0.7\times\hbar/a$, (b) $g_x=g_y=1.2\times\hbar/a$, (c) $g_x=g_y=1.5\times\hbar/a$, and (d) $g_x=g_y=4.0\times\hbar/a$.

plex energy. More generally, states related by a reflection across the **g** axis are degenerate. [In $d=3$, the degenerate states lie on a circle in (k_x,k_y,k_z) space centered on a line passing through **g**.] This degeneracy is split by the randomness. Degenerate perturbation theory requires diagonalization of the set of 2×2 matrices

$$\begin{pmatrix} \varepsilon_0(k_x,k_y) & \tilde{V}(k_x-k_y,k_y-k_x) \\ \tilde{V}(k_y-k_x,k_x-k_y) & \varepsilon_0(k_x,k_y) \end{pmatrix}, \tag{6.7}$$

where

$$\tilde{V}(k_a,k_b)\equiv\frac{1}{L_xL_y}\sum_{x,y} e^{ik_ax+ik_by}V_{x,y} \tag{6.8}$$

is the Fourier-transformed disorder potential and $\varepsilon_0(k_x,k_y)$ is given by Eq. (6.2). The eigenvalues of Eq. (6.7) are

$$\varepsilon_\pm(k_x,k_y)=\varepsilon_0(k_x,k_y)\pm\Delta, \tag{6.9}$$

where

$$\Delta\equiv|\tilde{V}(k_x-k_y,k_y-k_x)|. \tag{6.10}$$

The real splitting of the degenerate doublets predicted by Eq. (6.9) is clearly visible in Fig. 19(d).

The Bloch spectrum is only a good approximation provided these corrections are small compared to the spacing between the doublets. However, a typical spacing between the real parts of the Bloch levels for $L_x=L_y=L$ given by Eq. (6.2) is

$$\Delta\varepsilon\simeq\left|\frac{d\ \mathrm{Re}\varepsilon_0}{dk}\right|\Delta k\simeq 2ta\ \cosh\left(\frac{ga}{\hbar}\right)\frac{2\pi}{L}. \tag{6.11}$$

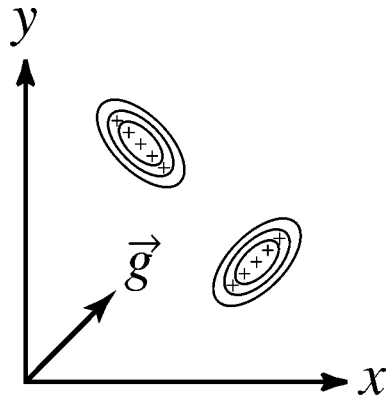

FIG. 20. Schematic view of two localized wave functions of the Hermitian system in two dimensions. The solid curves indicate contours on which the localized wave function takes the same value. The anisotropy arises because of anisotropic fluctuations in the impurity distribution. We show an impurity fluctuation that leads to two nearly degenerate wave functions related by a 90° rotation.

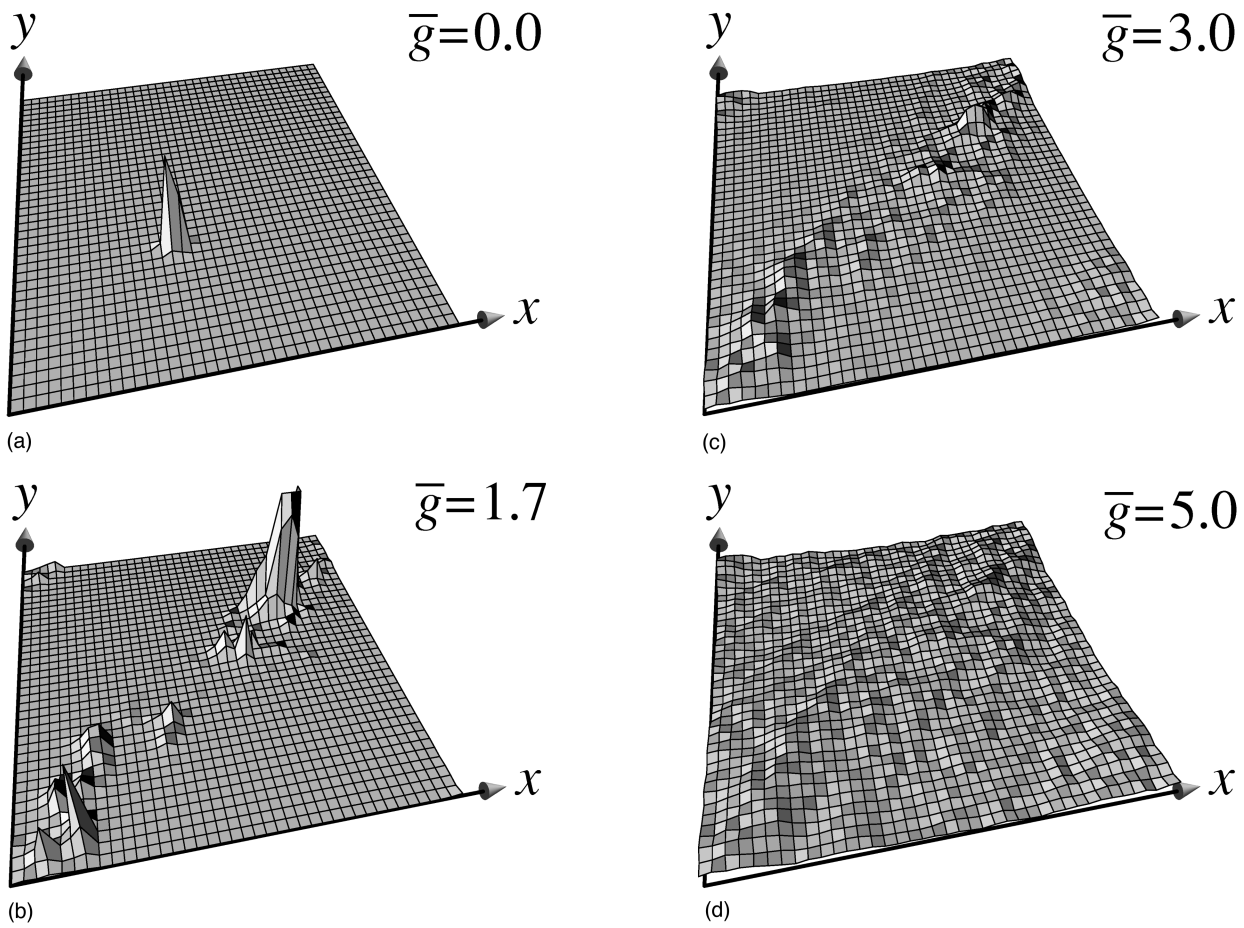

FIG. 21. Ground-state right eigenfunctions in two dimensions. We show the case $L_x=L_y=40a$ and $\Delta=10t$ with (a) $g_x=g_y=0$, (b) $g_x=g_y=1.7\times\hbar/a$, (c) $g_x=g_y=3.0\times\hbar/a$, and (d) $g_x=g_y=5.0\times\hbar/a$. The vertical scale was rescaled by 1/10 and 10 in (b) and (d), respectively. The highest peak in (b) was reduced in size for the visualization purposes.

The splitting Δ due to the randomness is thus only a small correction to the Bloch levels whenever

$$\frac{4\pi}{L}ta\,\cosh\left(\frac{ga}{\hbar}\right)>\Delta, \tag{6.12}$$

a condition that is *always* violated in sufficiently large systems as $L\to\infty$. When the inequality (6.12) is not satisfied, level repulsion interacts with the randomness in a complex way to produce chaotic spectra like that in Fig. 19(c). The Bloch states are nondegenerate in $d=1$, so this problem does not arise.

Some insight into the meaning of the chaotic eigenvalue spectra follows from tracking the ground-state wave function as a function of **g**. As shown in Fig. 21, the ground state first streaks out in the direction of **g**. (For very large **g**, the wave function eventually broadens to cover the entire lattice. However, as discussed above, we believe that this Bloch-wave behavior is an artifact of the small system size.) Arguments given in Ref. 5 show that the ground state can never be simply delocalized in the **g** direction while remaining localized in the perpendicular direction when $L\to\infty$. In Ref. 7 it is argued that the long-wavelength, low-frequency behavior of the non-Hermitian Schrödinger equation in $2+1$ dimensions for large **g** is described by a $(1+1)$-dimensional Burgers equation. The tilted flux lines described in this way wander away from the **g** direction to take advantage of exceptionally deep minima in the disorder potential. This mapping predicts a streaked-out but roughened ground-state wave function with roughness exponent 2/3.[7] At present, our system sizes are too small to provide a good quantitative check of this hypothesis.

For system small enough so that Bloch states are a good first approximation for large **g**, most states are approximately twofold degenerate as discussed above. However, for an $L\times L$ square lattice, there is a very large L-fold degeneracy for the state at the origin of the complex energy plane. Perturbation theory explains the removal of the degeneracy in the following way. We show that the first-order perturbation theory reduces to a diagonal one-dimensional random model, which is readily solved. We take the hopping term of Eq. (1.2) as the nonperturbative part and the random-potential term as the perturbation so that the zeroth-order spectrum may be given by Eq. (6.2) or Fig. 17. The zeroth-order wave functions $|k_x,k_y\rangle$ of the degenerate levels in question satisfy the relation $k_x-k_y=\pi/a$ (mod $2\pi/a$). The secular equation for the first-order perturbation of the degenerate levels consists of the matrix elements

$$\left\langle k_x,k_y\left|\sum_{\mathbf{x}}V_{\mathbf{x}}b_{\mathbf{x}}^{\dagger}b_{\mathbf{x}}\right|k_x',k_y'\right\rangle=\frac{1}{L^2}\sum_{x,y}e^{i(k_x-k_x')(x+y)}V_{x,y}, \tag{6.13}$$

where we used $k_y - k_y' = k_x - k_x'$ (mod $2\pi/a$). The above matrix elements are in fact equivalent to the momentum representation of the one-dimensional Hamiltonian

$$\mathcal{H}_{\rm eff} = \sum_{\xi} V_{\rm eff}(\xi) b_{\xi}^{\dagger} b_{\xi}, \tag{6.14}$$

where

$$V_{\rm eff}(\xi) \equiv \frac{1}{L} \sum_{\eta} V_{x,y}, \tag{6.15}$$

with $\xi \equiv x+y$ (mod L) and $\eta \equiv x-y$ (mod L). The effective potential (6.15) is thus obtained by integrating the original potential $V_{x,y}$ along a line parallel to **g**. The first-order perturbation spectrum is readily solved since the effective Hamiltonian (6.14) is already diagonalized. Thus we arrive at the first-perturbation energy

$$\varepsilon_{\xi}^{(1)} = V_{\rm eff}(\xi) \tag{6.16}$$

for $\xi = 0,1,\ldots,L-1$, which accounts for the horizontal spread of eigenvalues in Fig. 19(d).

VII. TRANSVERSE MEISSNER EFFECT AND ITS PENETRATION DEPTH

In this section we discuss the penetration depth associated with the transverse Meissner effect for superconductors with columnar defects in the localized regime. The vortex density is assumed to be finite. The surface deflection that defines the penetration depth for a *single* vortex line is shown in Fig. 15(a). We discuss only field penetration in directions parallel to the columns. For a more general discussion of various penetration depths, frequency dependences, etc., see Ref. 23.

As shown in Sec. IV B for the one-dimensional case, the displacement of the pinned flux line near the surface of the superconductor with one defect has, in general, an exponential τ dependence. The penetration depth τ^* has the singularity $\tau^* \sim \xi_{\perp} \sim (g-g_c)^{-1}$. We show below that the mean displacement at depth τ in the *many-defect* case in d dimensions is given by a stretched exponential form

$$\langle (\langle x \rangle_{\tau} - \langle x \rangle_{\infty}) \rangle_{\rm av} \underset{\tau \to \infty}{\sim} \exp[-a(\tau/\tau^*)^{1/(d+1)}], \tag{7.1}$$

where we now assume for simplicity that the field **g** is parallel to the x axis. The average displacement in directions perpendicular to **g** vanishes because of statistical symmetry. The quantity $\langle x \rangle_{\infty}$ is the center of the localized state in the bulk, which is identical to the average position of the corresponding state for $\mathbf{g}=\mathbf{0}$. Moreover, we show that the penetration depth has the singularity $\tau^* \sim \xi_{\perp}^z \sim (g_c - g)^{-z}$, with the dynamical exponent $z=d$, thus justifying Eqs. (1.8) and (1.9). Note that d is the dimensionality of the quantum system corresponding to flexible lines in $d+1$ dimensions.

Consider a low but finite density of interacting flux lines. As discussed in Sec. II, we fill up the localized states in order of increasing energy up to the average chemical potential $\varepsilon = \mu$. Consider the deflection of the most unstable (pinned) flux line near the surface. Since we forbid double occupancy of localized states, we can approximate

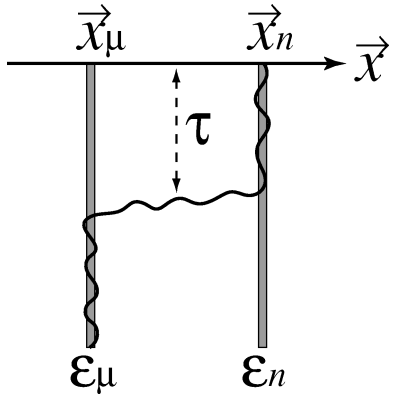

FIG. 22. Kink in a vortex configuration near the top surface of a superconducting sample.

$$\langle x \rangle_{\tau} \simeq \sum_{n}{}' c_n \int d^d\mathbf{x} \langle \psi_{\mu}|\mathbf{x}\rangle x \langle \mathbf{x}|\psi_n\rangle e^{-\tau \Delta\varepsilon_n/\hbar}, \tag{7.2}$$

where

$$c_n \equiv \frac{\int \langle \psi_n|\mathbf{x}'\rangle d^d\mathbf{x}'}{\int \langle \psi_{\mu}|\mathbf{x}'\rangle d^d\mathbf{x}'} \tag{7.3}$$

and

$$\Delta\varepsilon_n \equiv \varepsilon_n - \varepsilon_{\mu}, \tag{7.4}$$

in contrast to Eqs. (4.27), (4.28), and (4.29) appropriate to a single line. Here ψ_{μ} denotes an eigenstate at the chemical potential and the summation Σ_n' is restricted to states with the energies $\varepsilon \geqslant \mu$. Note that the coefficient c_n for an extended state will be quite small owing to oscillatory factors in the integration over the space. Because of the exponential factor in Eq. (7.2), the main contributions come from localized states near and above the chemical potential. We use the asymptotic form (3.5) for localized states to estimate Eq. (7.2). The term with $\psi_n = \psi_{\mu}$ gives $\langle x \rangle_{\infty}$. The other leading terms after the integration are approximately

$$|\langle x \rangle_{\tau} - \langle x \rangle_{\infty}| \simeq \sum_{n}{}'' \tilde{c}_n e^{-f_n(\tau)}, \tag{7.5}$$

where

$$f_n(\tau) \equiv [\hbar\kappa(\mu) - g\cos\theta_n] r_n + \tau\Delta\varepsilon_n/\hbar, \tag{7.6}$$

$r_n \equiv |\mathbf{x}_n - \mathbf{x}_{\mu}|$, $\cos\theta_n \equiv \mathbf{g}\cdot(\mathbf{x}_{\mu}-\mathbf{x}_n)/|\mathbf{g}|r_n$, and Σ_n'' is the summation over localized excited states with the energies $\varepsilon > \mu$. The inverse localization length κ_n was approximated by $\kappa(\mu)$. The new coefficient $\tilde{c}_n$ is $\tilde{c}_n \sim c_n r_n \cos\theta_n$. As in conventional Mott variable-range hopping in semiconductors,[24] we estimate the energy difference $\Delta\varepsilon_n$ from[10]

$$g(\mu) r_n^d \Delta\varepsilon_n \sim 1, \tag{7.7}$$

where $g(\mu)$ is the density of states at the chemical potential.

The quantity $f_n(\tau)$ gives the energy of a tilted flux-line configuration; see Fig. 22. The first term is the energy due to a kink joining columns at $\mathbf{x}_{\mu}$ and $\mathbf{x}_n$. Hence the energy is proportional to the width r_n of the kink. The second term is

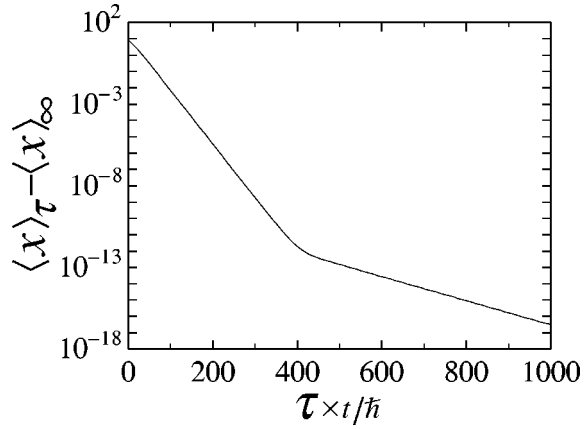

FIG. 23. τ dependence of the displacement of a flux line for a realization of randomness in the one-dimensional tight-binding model. Since only two terms of f_n contribute to the summation Σ_n'' in Eq. (7.5) in this example, the whole curve consists approximately of two lines. The slope of each line is $-\Delta\varepsilon_n/\hbar$, while its y intercept is $-(\hbar\kappa_n - g)r_n$. The parameters are $L_x = 500a$, $\Delta/t = 1$, and $g/t = 0.6$.

the energy loss arising because the flux line stays at $\mathbf{x}_n$ over the distance τ rather than at the most stable position $\mathbf{x}_\mu$. This energy loss is proportional to τ. Because of Eq. (7.7), the first and the second terms compete: The further the flux line hops from $\mathbf{x}_\mu$, the more the kink energy costs, but the lower the binding energy at $\mathbf{x}_n$. In variable-range hopping of electrons in semiconductors,[24] $\Delta\varepsilon_n$ is the energy difference between localized electronic states and the kink energy is replaced by a WKB tunneling matrix element.

Figure 23 shows the relaxation function $\langle x\rangle_\tau - \langle x\rangle_\infty$ for the one-dimensional tight-binding model with a particular realization of randomness. In this example, only two states contribute significantly to the summation Σ_n'' in Eq. (7.5). Upon averaging over many realizations of randomness (or close to the depinning transition), we expect contributions from many states as depicted schematically in Fig. 24. For a fixed τ, the largest contribution to the summation in Eq. (7.5) comes from the state at

$$r_n = \left(\frac{\tau d}{\hbar g(\mu)[\hbar\kappa(\mu) - g]} \right)^{1/(d+1)}, \tag{7.8}$$

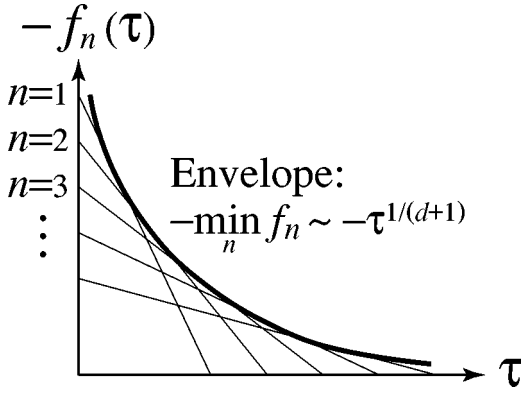

FIG. 24. Schematic of the situation where many different exponential terms contribute to the summation in Eq. (7.5).

which yields

$$\min_n f_n = a\left(\frac{\tau}{\tau^*} \right)^{1/(d+1)}, \tag{7.9}$$

with

$$\tau^* = \frac{\hbar g(\mu)}{[\hbar\kappa(\mu) - g]^d} \tag{7.10}$$

and $a = d^{1/(d+1)}(1 + 1/d)$. This gives the stretched exponential form (7.1). Since the displacement at the surface, or the surface transverse magnetization, is given by $\xi_\perp \sim M_{\perp s} \sim (\hbar\kappa - g)^{-1}$, we have $\tau^* \sim \xi_\perp^d$.

We obtain the stretched exponential form only in the limit $\tau \to \infty$. Deep in the Bose-glass phase, it may be difficult to observe this form experimentally because the amplitude of the surface displacement is small in this limit. However, the characteristic scale τ^* in the τ direction diverges, $\tau^* \sim [\hbar\kappa(\mu) - g]^{-d}$, where stretched-exponential relaxation should be relatively easy to observe.

VIII. EFFECT OF INTERACTIONS IN THE DELOCALIZED REGIME

A. 1+1 dimensions: Continuous phase transition

We conclude with a discussion of interaction effects. The delocalization transitions discussed above were treated using an independent-particle (or ''independent-vortex-line'') picture. As outlined above, interactions can be taken into account in the Bose-glass phase, provided that we forbid multiple occupancy of the localized states. The physics here is similar to the bands of localized impurity states describing electrons in disordered semiconductors.[24] In both Bose and Fermi glasses, localized states are filled in order of increasing energies up to a chemical potential. In the localized regime, the differences between Bose statistics of repelling flux lines interacting with columnar defects and Fermi statistics of electrons in disordered semiconductors are not expected to be important.[10]

Interactions must be handled differently in the delocalized phase. Consider what happens to the states described by the $(1+1)$-dimensional non-Hermitian spectra of Fig. 12(a) with increasing field $H_\parallel$ along the τ axis. We assume that the tilt field lies in a range such that there is a mobility edge separating low-energy localized states from high-energy delocalized ones. The field $H_\parallel$ controls the chemical potential of the equivalent disordered boson system.[10] As $H_\parallel$ increases, we fill the unoccupied levels in order of increasing energy to obtain the ground state. Eventually all states below the mobility edge are filled and additional vortices must then go into extended states above this boundary. These extended states describe macroscopically tilted vortex lines and as we can see from Fig. 13, the corresponding tilt slope is finite at the mobility edge. Interactions have a weaker effect on delocalized, tilted lines, so we expect that *many* lines can be accommodated by only a few delocalized states with energies just above the mobility edge. In the presence of thermal

fluctuations, there is not a sharp distinction between tilted and untilted lines; any individual line will be both tilted or localized in different regions along the τ axis. Alternatively, we can imagine that the delocalization transition happens at fixed $H_\parallel$, with increasing external tilt field $H_\perp$, as in Fig. 3.

A physical picture of the delocalized phase in $1+1$ dimensions in the presence of interactions has been developed by Hwa *et al.*[25] Tilted lines are represented by chains of kinks and the density of these chains goes *continuously* to zero with decreasing tilt field. Thus we predict that a continuous phase transition is possible, in contrast to arguments based on depinning of a single line, which suggest a first-order transition.[14] A phenomenon like Bose condensation describes the physics of the tilted fraction of the lines, consistent with many lines entering just a few extended states above the mobility edge. However, because phase fluctuations are so strong in $1+1$ dimensions, correlations of the boson parameter decay *algebraically* to zero at large distances instead of approaching a nonzero constant. There is also algebraic order in a translational order parameter associated with the density of tilted lines; the tilted phase is in fact a ''supersolid.''[25]

B. 2+1 dimensions: Existence of a phase transition

The physical picture of lines in the delocalized regime is more complicated in $2+1$ dimensions, as suggested by the intricate spectra for finite **g** displayed in Fig. 19. However, here again there is a range of intermediate tilt fields where only localized states exist at low energies. A ''mobility edge'' now separates real eigenvalues in the localized regime from a region along the real energy axis where extended and localized states *coexist*. Building up a ground state as in $1+1$ dimensions, we would expect some vortices to enter extended states describing tilted lines once the chemical potential (controlled by $H_\parallel$) crosses this mobility edge. A bosonic superfluid fraction of tilted lines will coexist with a ''normal fluid'' fraction of lines localized on columns. As in $1+1$ dimensions, however, any single line will participate in both ''fractions'' as it crosses a sufficiently thick sample. Although a *single* tilted line probably goes into a glassy ground state described by the Burgers equation,[7] interactions in a dense liquid of tilted lines can screen out random pinning potentials in a weakly perturbed superfluid phase of entangled lines.[13] The tilted liquid in this dense regime should be pinned only weakly and exhibit a linear resistivity.

If the tilted regime is entered by increasing $H_\perp$ at fixed $H_\parallel$, one is shifting the mobility edges in the $(2+1)$-dimensional spectra at fixed chemical potential. The sequence of possible phases probably resembles vortex matter subjected to point disorder near H_{c1}.[26] For small $H_\perp$, the Bose glass with its transverse Meissner effect resembles the usual Meissner phase for $H<H_{c1}$. Suppose now that $H_\perp$ is increased until $H_\perp>H_{\perp c}$ such that the lower mobility edge drops below the chemical potential. As illustrated in Fig. 3, one probably encounters a flux-liquid phase (with a finite fraction of tilted, entangled lines) if $H_\perp$ is increased at *high* temperatures. At low temperatures and large tilt fields, however, the stable phase is probably a crystalline vortex-smectic phase, where the tilted lines are arranged in sheets periodically spaced along the column direction to minimize the interaction energies.[27] Hwa *et al.*[25] have discussed a theory of how a continuous transition directly from this vortex smectic into the Bose glass might proceed. However, it is hard to rule out the possibility of a melted silver of tilted flux liquid at *all* nonzero temperatures when the density of tilted lines becomes very small near the transition curve $H_{\perp c}(T)$, similar to what happens in vortices subjected to point disorder near $H_{c1}(T)$. It is not yet known if a point disorder is sufficient to produce a distinct ''vortex-glass'' phase with a finite vortex density interposed between the flux liquid and the Meissner phase.[13] There are similar uncertainties about a distinct glassy phase near $H_{\perp c}(T)$ in the present problem.

Although we will not resolve these uncertainties here, we can show that there must be at least *one* phase transition separating a Bose glass at small $H_\perp$ from a tilted superfluid of entangled lines when $H_\perp$ is large. In other words, the transition suggested by the existence of a sharp mobility edge in the $(2+1)$-dimensional single-line spectra survives the imposition of repulsive interline interactions. We proceed by first noting that the tilt modulus

$$c_{44}\equiv\frac{B^2}{4\pi}\left(\frac{\partial B_\perp}{\partial H_\perp}\right)^{-1} \tag{8.1}$$

is divergent in the Bose-glass phase that results for small $H_\perp$.[10] This infinity is a consequence of the transverse Meissner effect: Although the lines tilt near the sample surfaces in response to a perpendicular external field (as in Fig. 22), there is no macroscopic response in an infinite sample, so $\partial B_\perp/\partial H_\perp=0$. We will show that the tilt modulus c_{44} remains *finite* in a superfluid liquid of entangled, tilted lines that results for $H_\perp>H_{\perp c}$, so that there *must* be at least one sharp phase transition as one increases $H_\perp$. The tilt modulus is proportional to the inverse superfluid density of the equivalent boson system and the corresponding results for the superfluid density ρ_s are indicated in Fig. 3.

We start with the generalization of Eq. (2.1) for N lines $\{\mathbf{x}_j(\tau)\}$, namely,[10]

$$E_{\rm flux}[\{\mathbf{x}_j(\tau)\}]\equiv\frac{\tilde{\varepsilon}_1}{2}\sum_{j=1}^{N}\int_0^{L_\tau}d\tau\left[\left(\frac{d\mathbf{x}_j}{d\tau}\right)^2-\mathbf{g}\cdot\frac{d\mathbf{x}_j}{d\tau}+V[\mathbf{x}_j(\tau)]\right]$$

$$+\frac{1}{2}\sum_{i\neq j}\int_0^{L_\tau}d\tau V_{\rm int}[|\mathbf{x}_i(\tau)-\mathbf{x}_j(\tau)|], \tag{8.2}$$

where $\mathbf{g}\equiv\phi_0\mathbf{H}_\perp/4\pi$ and we have added a repulsive potential $V_{\rm int}$ between the lines. We neglect point disorder and assume for simplicity that the columnar pinning potential is weak or the temperature is fairly high, so that the transition out of the Bose glass occurs for relatively small values of $\mathbf{g}\propto\mathbf{H}_\perp$. The assumptions of small line tilts and local (in τ) interactions between flux lines that justify Eq. (8.2) (Ref. 10) are then

satisfied even for $H_\perp > H_{\perp c}$. The many-line partition function associated with Eq. (8.2) is

$$\mathcal{Z}(\mathbf{g}) \equiv \prod_{j=1}^{N} \int \mathcal{D}\mathbf{x}_j(\tau) e^{-E_{\rm flux}[\{\mathbf{x}_j(\tau)\}]/k_B T}. \tag{8.3}$$

Upon defining an operator $\mathbf{X}_{\rm op} \equiv \sum_{j=1}^{N} \mathbf{x}_j^{\rm op}$ acting on position eigenstates $|\mathbf{x}_1,\ldots,\mathbf{x}_N\rangle$ such that

$$\mathbf{X}_{\rm op}|\mathbf{x}_1,\ldots,\mathbf{x}_N\rangle = \left(\sum_{j=1}^{N} \mathbf{x}_j\right)|\mathbf{x}_1,\ldots,\mathbf{x}_N\rangle, \tag{8.4}$$

standard manipulations allow us to write this multidimensional path integral in terms of a quantum-mechanical matrix element

$$\mathcal{Z}(\mathbf{g}) = \int d^2\mathbf{r}_1' \cdots d^2\mathbf{r}_N' \int d^2\mathbf{r}_1 \cdots d^2\mathbf{r}_N \langle \mathbf{r}_1' \cdots \mathbf{r}_N' | e^{\mathbf{g}\cdot\mathbf{X}_{\rm op}/(k_B T)} e^{-\mathcal{H}(\mathbf{0})L_\tau/k_B T} e^{-\mathbf{g}\cdot\mathbf{X}_{\rm op}/(k_B T)} | \mathbf{r}_1 \cdots \mathbf{r}_N \rangle, \tag{8.5}$$

where the ''Hamiltonian'' $\mathcal{H}(\mathbf{0})$ is

$$\mathcal{H}(\mathbf{0}) = -\frac{(k_B T)^2}{2\tilde{\varepsilon}_1} \sum_{j=1}^{N} \nabla_j^2 + \sum_{j=1}^{N} V[\mathbf{x}_j] + \frac{1}{2} \sum_{i \neq j} V_{\rm int}(|\mathbf{x}_i - \mathbf{x}_j|). \tag{8.6}$$

Upon noting that

$$\begin{aligned} & e^{\mathbf{g}\cdot\mathbf{X}_{\rm op}/(k_B T)} e^{-\mathcal{H}(\mathbf{0})L_\tau/k_B T} e^{-\mathbf{g}\cdot\mathbf{X}_{\rm op}/k_B T} \\ &= \sum_{n=0}^{\infty} \frac{1}{n!} e^{\mathbf{g}\cdot\mathbf{X}_{\rm op}/k_B T} \left(-\frac{\mathcal{H}(\mathbf{0})L_\tau}{k_B T}\right)^n e^{-\mathbf{g}\cdot\mathbf{X}_{\rm op}/k_B T} \\ &= e^{-\mathcal{H}(\mathbf{g})L_\tau/k_B T}, \end{aligned} \tag{8.7}$$

where

$$\begin{aligned} \mathcal{H}(\mathbf{g}) &= e^{\mathbf{g}\cdot\mathbf{X}_{\rm op}/k_B T} \mathcal{H}(\mathbf{0}) e^{-\mathbf{g}\cdot\mathbf{X}_{\rm op}/k_B T} \\ &= \frac{1}{2\tilde{\varepsilon}_1} \sum_{j=1}^{N} \left(\frac{k_B T}{i}\nabla_j + i\mathbf{g}\right)^2 + \sum_{j=1}^{N} V[\mathbf{x}_j] \\ &\quad + \frac{1}{2} \sum_{i \neq j} V_{\rm int}(|\mathbf{x}_i - \mathbf{x}_j|), \end{aligned} \tag{8.8}$$

and referring to Table I, we see that this Hamiltonian is the generalization of Eq. (1.1) for many interacting vortex lines.

Note that if a many-body eigenfunction $\Psi_n(\mathbf{x}_1,\ldots,\mathbf{x}_N;\mathbf{0})$ of $\mathcal{H}(\mathbf{g}=\mathbf{0})$ for localized lines in the Bose glass phase is known, a potentially exact right eigenfunction with the same energy for $\mathbf{g} \neq \mathbf{0}$ is then

$$\Psi_n^R(\mathbf{x}_1,\ldots,\mathbf{x}_N;\mathbf{g}) = e^{\mathbf{g}\cdot\mathbf{X}_{\rm op}/k_B T} \Psi_n(\mathbf{x}_1,\ldots,\mathbf{x}_N;\mathbf{0}), \tag{8.9}$$

as follows immediately from the first line of Eq. (8.8). As in the single-particle case, this gauge transformation connecting the $\mathbf{g}=\mathbf{0}$ and $\mathbf{g}\neq\mathbf{0}$ problems only works provided that the new eigenfunction is normalizable.[17]

To treat the tilted phase of entangled lines, it is convenient to modify the original path-integral partition function via the change of variables

$$\mathbf{x}_j(\tau) = \mathbf{x}_j'(\tau) + \frac{\mathbf{g}}{\tilde{\varepsilon}_1}\tau. \tag{8.10}$$

Upon transforming to a quantum-mechanical matrix element as before, we arrive at

$$\mathcal{Z}(\mathbf{g}) = \int d^2\mathbf{r}_1' \cdots d^2\mathbf{r}_N' \int d^2\mathbf{r}_1 \cdots d^2\mathbf{r}_N \left\langle \mathbf{r}_1' \cdots \mathbf{r}_N' \middle| T \exp\left(-\frac{1}{k_B T}\int_0^{L_\tau} \mathcal{H}'(\mathbf{g};\tau) d\tau\right) \middle| \mathbf{r}_1 \cdots \mathbf{r}_N \right\rangle, \tag{8.11}$$

with

$$\begin{aligned} \mathcal{H}'(\mathbf{g};\tau) &= -\frac{(k_B T)^2}{2\tilde{\varepsilon}_1} \sum_{j=1}^{N} \nabla_j^2 + \sum_{j=1}^{N} V'[\mathbf{x}_j,\tau] \\ &\quad + \frac{1}{2} \sum_{i \neq j} V_{\rm int}(|\mathbf{x}_i - \mathbf{x}_j|), \end{aligned} \tag{8.12}$$

where the constant imaginary vector potential is missing, but $V[\mathbf{x}_j]$ has been replaced by a τ-dependent disorder potential

$$V'[\mathbf{x}_j,\tau] \equiv V\left[\mathbf{x}_j + \frac{\mathbf{g}}{\tilde{\varepsilon}_1}\tau\right]. \tag{8.13}$$

The symbol T in front of the exponential in Eq. (8.11) stands for time ordering. The above new Hamiltonian [related to Eq. (8.8) via an imaginary Galilean transformation[13]] describes a set of vortex lines moving along the τ axis in the presence of a set of parallel, tilted columnar defects. The response functions for a liquid of interacting entangled lines in the presence of tilted disorder have been discussed and reviewed by Täuber and Nelson.[19] The vortex tilt moduli both parallel and perpendicular to the plane of tilt in this case are different. However, both are explicitly found to be *finite*, in contrast to the infinite tilt moduli in the Bose glass. Thus there must indeed be at least one genuine phase transition for the $(2+1)$-dimensional system with increasing $\mathbf{H}_\perp \propto \mathbf{g}$ in the presence of interactions and disorder.

ACKNOWLEDGMENTS

The authors are grateful to Nadav Shnerb for many helpful comments and discussions, as well as for conversations with B. I. Halperin and J. Wang. This research was supported by the National Science Foundation through Grant No. DMR94-17047 and by the Harvard Materials Research Science and Engineering Laboratory through Grant No. DMR94-00396. N.H. wishes to thank the Nishina Foundation for financial support during his stay at Harvard University.

APPENDIX: EXACT SOLUTION OF THE ONE-DIMENSIONAL SCHRÖDINGER EQUATION WITH A POINT IMPURITY

In this appendix we describe the derivation of the single-impurity results given in Sec. IV A. The derivation is subtle even in the Hermitian case, since we are interested in finite-size effects as well as the thermodynamic limit. Throughout this appendix we assume $g>0$ without loss of generality.

We have found it useful to solve the Schrödinger equation $\mathcal{H}\psi^R(x)=\varepsilon\psi^R(x)$ in a way different from that sketched in Ref. 5. Because of the periodic boundary conditions (4.2), we define the Fourier transformation in the form

$$\psi^R(x)=\frac{2\pi}{L_x}\sum_k \tilde{\psi}^R(k)e^{ikx}, \tag{A1}$$

where the summation runs over $k=2\pi n/L_x$ for integer n. The inverse transformation is given by

$$\tilde{\psi}^R(k)=\frac{1}{2\pi}\int_0^{L_x}\psi^R(x)e^{-ikx}dx. \tag{A2}$$

The Schrödinger equation becomes

$$(\hbar k+ig)^2\tilde{\psi}^R(k)-\frac{mV_0}{\pi}\psi^R(0)=2m\varepsilon\tilde{\psi}^R(k). \tag{A3}$$

Upon assuming that $C\equiv\psi^R(0)$ is finite, we have

$$\tilde{\psi}^R(k)=\frac{mV_0C}{\pi\hbar^2}\left[\left(k+i\frac{g}{\hbar}\right)^2-K^2\right]^{-1}, \tag{A4}$$

where $K(\varepsilon)\equiv\sqrt{2m\varepsilon}/\hbar$. The real-space wave function is given by substituting $\tilde{\psi}^R(k)$ in Eq. (A1) with Eq. (A4).

The condition $\psi^R(0)=C$ results in the equation for the energy spectrum ε, namely,

$$\frac{2\pi}{L_x}\sum_k\left[\left(k+i\frac{g}{\hbar}\right)^2-K^2(\varepsilon)\right]^{-1}=\frac{\pi\hbar^2}{mV_0}. \tag{A5}$$

Let us first analyze this equation in the limit $L_x\to\infty$:

$$\int_{-\infty}^{\infty}dk\left[\left(k+i\frac{g}{\hbar}\right)^2-K^2(\varepsilon)\right]^{-1}=\frac{\pi\hbar^2}{mV_0}. \tag{A6}$$

The integrand has two poles at $k=\pm K-ig/\hbar$ in the complex plane of k. For $|\mathrm{Im}\,K|<g/\hbar$, the integral (A6) vanishes when we close the integration contour in the upper half plane. Thus nonzero solutions arise only for $|\mathrm{Im}K|\geq g/\hbar$. In the following, we derive solutions for $|\mathrm{Im}K|>g/\hbar$ and for $|\mathrm{Im}K|=g/\hbar$ separately.

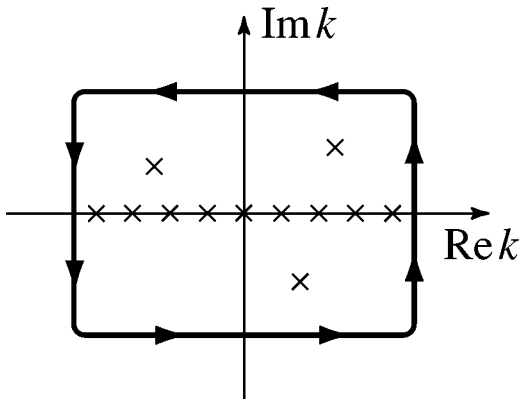

FIG. 25. Integration contour used in the evaluation of Eq. (A10). The crosses on the horizontal axis indicate the poles of the factor $(e^{iLz}-1)^{-1}$, while the other two crosses indicate the poles of the function $R(z)$.

For $|\mathrm{Im}K|>g/\hbar$, the poles straddle the real axis and we have

$$\frac{\pi i}{K}=\frac{\pi\hbar^2}{mV_0} \tag{A7}$$

or

$$K=i\frac{mV_0}{\hbar^2}\equiv i\kappa_{\mathrm{g.s.}}. \tag{A8}$$

Thus we arrive at the unique localized ground-state solution for $|\mathrm{Im}K|>g/\hbar$ given as Eq. (4.4). The boundary for the existence of this localized state is the critical field, which leads to Eq. (4.3).

For $\mathrm{Im}K=g/\hbar$, one of the poles of the integrand of Eq. (A6) approaches the real k axis, which makes the evaluation of the integral in the limit $L_x\to\infty$ difficult. Hence we return to Eq. (A5) and explore the solutions including finite-size corrections, using the formula

$$\frac{2\pi}{L}\sum_{n=-\infty}^{\infty}R\left(\frac{2\pi}{L}n\right)=-\sum_{\zeta}\ \mathrm{Res}\left(R(z)\frac{2\pi i}{e^{iLz}-1};\zeta\right), \tag{A9}$$

where $R(z)$ is a rational function with the conditions that (i) the order in z of the denominator is greater than the order of the numerator at least by 2 and (ii) the function does not have any poles at integral points. The summation with respect to ζ runs over the residues arising from all poles of $R(z)$. The formula follows from evaluating

$$\oint dz\ R(z)\frac{2\pi i}{e^{iLz}-1}, \tag{A10}$$

with the integration contour as in Fig. 25. Thus Eq. (A5) becomes

$$(e^{iKL_x+L_xg/\hbar}-1)^{-1}-(e^{-iKL_x+L_xg/\hbar}-1)^{-1}=\frac{i\hbar^2K}{mV_0} \tag{A11}$$

or

$$K\left[\cosh\left(L_x\frac{g}{\hbar}\right)-\cos(L_xK)\right]+\frac{mV_0}{\hbar^2}\sin(L_xK)=0. \tag{A12}$$

The wave function corresponding to each solution of Eq. (A11) is

$$\psi^R(x)\propto\frac{e^{iKx+xg/\hbar}}{e^{iKL_x+L_xg/\hbar}-1}-\frac{e^{-iKx+xg/\hbar}}{e^{-iKL_x+L_xg/\hbar}-1} \tag{A13}$$

for $0\leqslant x<L_x$. In the case of $\lim_{L_x\to\infty}\mathrm{Im}K(L_x)>g/\hbar$, putting K to be pure imaginary results in the ground-state solution (A8) and (4.7) for $g<g_c$ in the limit $L_x\to\infty$.

We are now in a position to discuss the case

$$\lim_{L_x\to\infty}\mathrm{Im}K(L_x)=\frac{g}{\hbar}, \tag{A14}$$

where $K(L_x)$ denotes a solution of Eq. (A12). This case includes all delocalized wave functions. By setting

$$K(L_x)=k(L_x)+i\frac{g}{\hbar}+i\,\delta\kappa(L_x), \tag{A15}$$

with

$$\lim_{L_x\to\infty}\delta\kappa(L_x)=0, \tag{A16}$$

Eq. (A11) becomes

$$L_x\frac{g}{\hbar}e^{-w}\simeq L_x\left(\frac{g}{\hbar}-\frac{g_c}{\hbar}\right)+w \tag{A17}$$

in the limit $L_x\to\infty$, where

$$w\equiv L_x\delta\kappa(L_x)-iL_xk(L_x). \tag{A18}$$

We notice that $\kappa(L_x)$ and $k(L_x)$ have the same order of magnitude with respect to L_x.

For $g\neq g_c$, the second term on the right-hand side of Eq. (A17) is negligible compared to its first term and hence

$$w\simeq\ln\frac{g}{g-g_c}. \tag{A19}$$

This gives a series of solutions in addition to the ground state (A8). For $g<g_c$, we have

$$L_x\delta\kappa=\ln\frac{g}{g_c-g}, \tag{A20}$$

$$L_xk=\ln(-1)=i\pi(2n+1), \tag{A21}$$

with n an integer, i.e., the excited states given in Eqs. (4.10) and (4.11). For $g>g_c$, we have

$$L_x\delta\kappa=\ln\frac{g}{g-g_c}, \tag{A22}$$

$$L_xk=\ln 1=2i\pi n, \tag{A23}$$

or the excited states given in Eqs. (4.14) and (4.15). Finally, for $g=g_c$, Eq. (A17) yields a solution $w=O(\ln L_x)$, or Eq. (4.19).

*Present address: Theoretical Division, Los Alamos National Laboratory, Los Alamos, NM 87545.

[1] L. P. Kadanoff and J. Swift, Phys. Rev. **165**, 310 (1968).
[2] H. C. Fogedby, A. B. Eriksson, and L. V. Mikheev, Phys. Rev. Lett. **75**, 1883 (1995).
[3] D. Kim, Phys. Rev. E **52**, 3512 (1995).
[4] B. M. McCoy and T. T. Wu, Nuovo Cimento B **56**, 311 (1968); see also E. H. Lieb and F. Y. Wu, in *Phase Transitions and Critical Phenomena Vol. 1*, edited by C. Domb and M. S. Green (Academic, London, 1972), p. 331.
[5] N. Hatano and D. R. Nelson, Phys. Rev. Lett. **77**, 570 (1996).
[6] For a review see *The Quantum Hall Effect*, 2nd ed., edited by R. E. Prange and S. M. Girvin (Springer-Verlag, New York, 1990).
[7] D. R. Nelson and N. Shnerb, cond-mat/9708071 (unpublished).
[8] L. Civale, A. D. Marwick, T. K. Worthington, M. A. Kirk, J. R. Thompson, L. Krusin-Elbaum, Y. Sun, J. R. Clem, and F. Holtzberg, Phys. Rev. Lett. **67**, 648 (1991).
[9] R. C. Budhani, M. Suenaga, and S. H. Liou, Phys. Rev. Lett. **69**, 3816 (1992).
[10] D. R. Nelson and V. Vinokur, Phys. Rev. B **48**, 13 060 (1993).
[11] L. Balents and D. R. Nelson, Phys. Rev. B **52**, 12 951 (1995).
[12] M. P. A. Fisher, P. B. Weichman, G. Grinstein, and D. S. Fisher, Phys. Rev. B **40**, 546 (1989).
[13] D. R. Nelson and P. Le Doussal, Phys. Rev. B **42**, 10 113 (1990).
[14] L.-W. Chen, L. Balents, M. P. A. Fisher, and M. C. Marchetti, Phys. Rev. B **54**, 12 798 (1996).
[15] J. Miller and J. Wang, Phys. Rev. Lett. **76**, 1461 (1996).
[16] M. C. Marchetti and V. M. Vinokur, Phys. Rev. B **51**, 16 276 (1995).
[17] P. Le Doussal (unpublished); see also Sec. IV D of Ref. 10.
[18] The Frobenius-Perron theorem ensures that the ground state is nodeless and nondegenerate with a real eigenvalue even in this non-Hermitian problem. See, e.g., F. R. Gantmacher, *The Theory of Matrices, Vol. 2* (Chelsea, New York, 1974).
[19] U. Täuber and D. R. Nelson, Phys. Rep. (to be published).
[20] J. T. Edwards and D. J. Thouless, J. Phys. C **5**, 807 (1972).
[21] D. C. Liccardello and D. J. Thouless, J. Phys. C **8**, 4157 (1975).
[22] A study of Hermitian localization has suggested a diverging localization length κ precisely at the band center for another type of the probability distribution. In this case, the state with $\varepsilon=0$ for $g=0$ is delocalized as soon as g becomes nonzero. See M. O. Robbins and B. Koiller, Phys. Rev. B **32**, 4576 (1985).
[23] D. R. Nelson and L. Radzihovsky, Phys. Rev. B **54**, 6845 (1996).
[24] B. I. Shklovskii and A. L. Efros, *Electronic Properties of Doped Semiconductors* (Springer-Verlag, New York, 1984).
[25] T. Hwa, D. R. Nelson, and V. M. Vinokur, Phys. Rev. B **48**, 1167 (1993). [See Fig. 5 of this reference for a schematic of $(1+1)$-dimensional tilted vortex lines in the presence of columnar pins.]
[26] See Sec. IV C of Ref. 13 for a discussion of vortex lines with disorder near H_{c1}.
[27] See Appendix A of Ref. 10.